Deep-Sea Research Part II xxx (xxxx) xxx–xxx

Contents lists available at ScienceDirect

Deep-Sea Research Part II

journal homepage: www.elsevier.com/locate/dsr2

Deposition patterns on the Chukchi shelf using radionuclide inventories in relation to surface sediment characteristics

Lee W. Cooper*, Jacqueline M. Grebmeier

Chesapeake Biological Laboratory, University of Maryland Center for Environmental Science, PO Box 38, Solomons, MD 20688, USA

ARTICLE INFO

Keywords:
Sedimentation
Chukchi Sea
East Siberian Sea
Radiocesium
Lead-210

ABSTRACT

Forty sediment cores collected on the Chukchi shelf and adjacent portions of the East Siberian Sea have been assayed for the sedimentation tracer ^{137}Cs and 34 were also assayed for ^{210}Pb. While both sedimentation and bioturbation influence how these tracers are distributed vertically in sediment cores, only about half of the cores had distinct, single mid-depth or subsurface maximum activity peaks associated with ^{137}Cs originating from bomb fallout. For the same reasons, only 14 of the 34 cores assayed showed a consistent decline in excess sedimentary ^{210}Pb with depth in the core. Furthermore, sedimentation rate estimates from ^{210}Pb assays were only consistent with estimated ^{137}Cs sedimentation rates in 4 of the 14 cores from north of Bering Strait. A high degree of bioturbation on the shelf is primarily responsible for these patterns, but the influence of sedimentation on vertical profiles is also important, particularly in areas of low accumulation where shallow burial of maximum burdens of ^{137}Cs in high current areas such as Herald Canyon can be observed. Shallow burial of radiocesium is also observed in comparatively low sedimentation areas such as Hanna Shoal, on the northeast Chukchi Shelf. By contrast, elsewhere on the northeast Chukchi Shelf and in productive benthic "hotspots," the stronger influence of bioturbation leads to radiocesium that is more evenly distributed vertically within sediments, i.e., no distinct mid- or subsurface depth maximum activity associated with bomb fallout. These sediment profiles of radiocesium reflect several other sediment characteristics that are affected by current flow. These sediment characteristics in turn impact biological activity, including grain size, carbon to nitrogen ratios of the organic fraction of surface sediments and total organic carbon content. The distribution patterns of the radionuclides, particularly the depth where ^{137}Cs reaches maximum activity, reflects sedimentation under both quiescent and strong currents. The activity of ^{137}Cs at that depth of maximum activity provide insights on how much the vertical distribution of the radionuclide has been impacted by bioturbation, as well as the characteristics of the sediments that play a role in influencing deposition and total inventories of radiocesium on continental shelves.

1. Introduction

Sedimentation rates and associated processes that control the accumulation of materials on the sea floor are critical to understanding linkages between pelagic and benthic systems (Hargrave, 1973; Grebmeier et al., 1988). Radionuclides such as ^{137}Cs and ^{210}Pb can be used in many circumstances to help improve our understanding of links to water column sedimentation and burial of potential contaminants [e.g. Koide et al. (1972); Robbins and Edgington (1975); Smith and Walton (1980)]. On shelves in the North American Arctic, recognition of strong pelagic-benthic coupling between seasonally productive water column and underlying shallow, broad shelves has led to several prior studies documenting sedimentation rates and accumulation patterns of specific radionuclides (e.g. Baskaran and Naidu, 1995; Cooper et al., 1998a; Cooper et al., 2005, Pirtle-Levy et al., 2009; Oguri et al., 2012; Trefry et al., 2014).

We expand on these earlier studies here by presenting radionuclide data from 40 cores collected at a wide variety of locations on the Chukchi and East Siberian shelves during programs supported by the US National Oceanic and Atmospheric Administration (the Russian-American Long-term Census of the Arctic—RUSALCA), and the US Bureau of Ocean Energy Management (Chukchi Sea Offshore Monitoring in Drilling Area —COMIDA Chemistry and Benthos and COMIDA Hanna Shoal). Each of these programs had different goals. For example, the COMIDA program, concerned about the fate of contaminants associated with oil and gas drilling on the Chukchi Shelf, required a better understanding of the dynamics and depth of bioturbation in shelf sediments to determine how long contaminants might

* Corresponding author.
E-mail address: cooper@umces.edu (L.W. Cooper).

https://doi.org/10.1016/j.dsr2.2018.01.009

persist near the sediment surface. The RUSALCA program was motivated by the need for better understanding of arctic biodiversity, so determining the relationship of overlying water production on the structuring of marine benthic communities and associated sediment characteristics was important. In the data presentations, a hyphen following the station name (e.g. UTX8-) precedes the station number (40 in UTX8-40) for the 2009 and 2013 cruises that were supported through the COMIDA program. RUSALCA stations are simply presented by name (e.g. HC22).

1.1. Radionuclide sources and distributions

We used the two widely used radioisotopes mentioned above, ^{137}Cs and ^{210}Pb, to meet these individual project objectives. ^{137}Cs is a bomb fallout product (30.2 year half-life) with a maximum deposition on the Earth's surface coinciding with the signing of the Limited Nuclear Test Ban Treaty in 1963, which ended most atmospheric nuclear weapons testing. Other secondary sources include the Chernobyl and Fukushima–Daiichi nuclear plant accidents, point pollution sources such as the La Hague (France) and Sellafield (UK) nuclear fuel cycle reprocessing plants, nuclear weapons manufacturing and waste generation facilities such as Hanford (Columbia River, USA) and Zheleznogorsk (Yenisei River, Russia). As an alkali metal, cesium is highly soluble in water and most radiocesium in the world ocean remains dissolved. It reaches the sediments through (1) sorption on clay particles in soils that are eroded into the ocean, (2) uptake or authigenesis at the sediment-water interface, and (3) biological uptake (Noshkin and Bowen, 1973; Livingston and Bowen, 1979; Ritchie and McHenry, 1990; Avery, 1996). The depth of penetration of the radionuclide and the distribution of the radioisotope in sediments reflects both sedimentation rates and bioturbation because no ^{137}Cs was present on Earth prior to development of nuclear weapons in the late 1940s. Given the stratospheric bomb fallout maximum in 1963–1964, a sedimentation rate can be estimated, where bioturbation has not obscured the maximum, by dividing the sediment depth where the radiocesium peak occurs by the number of years between core collection and 1964. We define sedimentation broadly here to include re-distribution of ^{137}Cs on fine clay particles during re-suspension events or transport by bottom boundary currents as well as the initial sedimentation of the isotope from bomb fallout. The available evidence from the Bering and Chukchi shelf and slope (e.g. Pirtle-Levy et al., 2009) suggests initial sedimentation is usually more important than re-suspension events because mid-depth or sub-surface maxima in radiocesium are preserved in many cores, and most cores outside of areas with known high bioturbation also show lower activities in recent years in the surface increments of the cores.

^{210}Pb is another independent tracer of sedimentation (Koide et al., 1972). It is a natural radioisotope (22.3 year half-life) that is a daughter product of the ^{238}U decay series. Some ^{210}Pb is present that falls to the Earth's surface because one of the immediate precursors to ^{210}Pb in the uranium decay series is the radioactive gas ^{222}Rn. Sedimentation studies of this radionuclide require determining the “supported” or background activities of ^{210}Pb in the sediments by determining an inventory of the radionuclide present naturally without considering the contributions of “excess” ^{210}Pb that is derived from atmospheric deposition (as radon decays). Once the supported ^{210}Pb inventory has been determined, a sedimentation rate can be estimated by plotting the logarithm of the excess ^{210}Pb activity against the mid-depth point of each core increment where ^{210}Pb declines steadily with depth. The decay constant for ^{210}Pb we use here is -0.01352 year^{-1} for convenience with plots of base 10 logarithms of excess activity (-0.031 yr^{-1} can be used alternatively for the natural log of excess activity that reflects the 22.3 year half-life). This activity coefficient is then divided by the calculated slope of this line relating sediment depth to the logarithm of the excess activity. Expressed as a formula, sedimentation is estimated from the best-fit equation,

$$\textit{sedimentation rate} = \lambda / b$$

where λ is the ^{210}Pb decay constant (-0.01352; for data plotted logarithmically) and b is the slope of the best-fit equation relating log excess radioactivity to the mid-point of each depth increment in the regression. Activity in the surface mixed layer, and below the point at which ^{210}Pb activities decline to a background level supported by in-situ radioactive decay are excluded from the calculated slope.

1.2. Synthesis with other available data

In addition to the specific radionuclide data that we present here, large data sets documenting other sediment characteristics have become available on the Chukchi Shelf within the past decade, including distributions of grain size, organic content and elemental and isotopic ratios of that organic content, sediment chlorophyll inventories as a function of settling organic matter, benthic biomass, taxonomic distributions and other indicators (e.g. Grebmeier et al., 2006; Dunton et al., 2012; Grebmeier and Cooper, 2014; Grebmeier and Cooper, 2016; Cooper et al., 2015; Grebmeier et al., 2015). Many of these sediment characteristics vary in response to water masses that influence productivity and sedimentation, which can in turn impact bioturbation within the sediments by supporting benthic communities. In addition, the intensity of flow northward across the shelf also plays a key role in structuring benthic biological communities, which can be dominated by epibenthic filter feeders in areas of high current flow (Bluhm et al., 2009; Pisareva et al., 2015), or infaunal macrofaunal communities where deposition of organic materials sustains deposit feeding benthic organisms (Grebmeier et al., 2015).

In this study, we synthesize some of the available data sets from the Chukchi Shelf to determine whether the characteristics of surficial sediments and benthic communities are coupled closely to insights provided by direct sedimentation measurements provided by radionuclide profiles. The synthesis challenge that we sought to address in this study was whether the large and diverse data sets that have become available for the Chukchi Shelf sediment characteristics and benthic communities could be linked to the measurements of direct sedimentation provided by the radionuclides studied. Sedimentation is modulated by bioturbation, which is a function of benthic biological activity. Characteristics of flow and currents across the broad shelf also impact the sedimentation of materials to the sea floor, while also influencing the structure of benthic biological communities. We use these sediment data that were acquired on the same research cruises where the sedimentation cores were collected in order to explore these complexities.

The sediment characteristics that were evaluated in the context of the sedimentation studies undertaken with the radionuclides included sediment grain size, C/N ratios and total organic carbon (TOC) in surface sediments, and the inventories of sediment chlorophyll present in surface sediments. On the Chukchi Shelf, the predominance of fine sediment grain sizes is one of the single best key predictors for biomass of benthic biological community structure (Grebmeier et al., 2006), which would be expected to influence the depth and degree of bioturbation. TOC in surface sediments is interrelated with benthic productivity and is also a significant predictor of benthic biomass (Grebmeier et al., 2006). In addition, TOC is an indicator of current flow regimes, with higher TOC associated with slower current speeds (Pisareva et al., 2015). Significantly, on the Chukchi Shelf, activities of ^{137}Cs, which is preferentially bound to clay mineral surfaces, are also related to fine sediment content and TOC, (Cooper et al., 1998a) so it should be expected that regional variation in the total inventories of radiocesium in sediments will be related in part to current regimes through their influence on fine particle deposition. C/N ratios in the organic fraction of surface sediments provide an index of food quality reaching the sea floor with lower C/N ratios reflecting areas of enhanced marine deposition of pelagic marine production (Grebmeier and McRoy, 1989; Grebmeier et al., 2006). Finally, the inventory of active chlorophyll

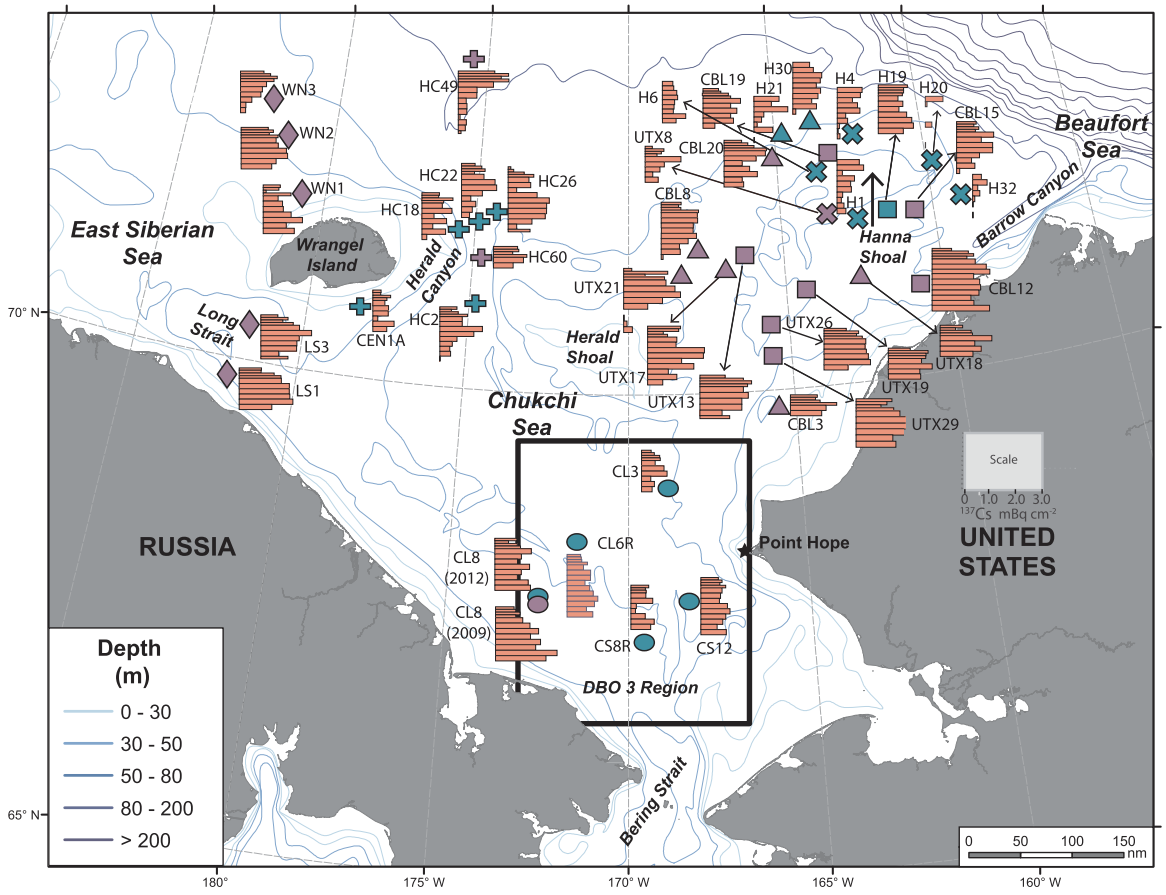

Fig. 1. Location of the cores studied in the Chukchi Sea and adjacent East Siberian Sea. Symbol key: Circles are cores collected in the DBO3 high productivity area; triangles are cores from the northeast Chukchi Sea with subsurface radiocesium maxima; x-shaped symbols are cores collected from Hanna Shoal, defined as water depths < 45 m; squares are cores from the northeast Chukchi Sea that appear to be more influenced by bioturbation and generally lack prominent subsurface maxima; crosses are collected from the Herald Canyon region; and diamonds are cores collected from Long Strait and the East Siberian Sea. Purple symbols are cores collected in 2009 and green symbols are cores collected in 2013. Station names are adjacent to the symbols, but station names associated with the COMIDA programs are simplified for ease of placement on the figure and include only the station name and not a hyphen followed by the COMIDA station number (see Introduction for station name convention). The miniaturized, equally scaled profiles shown for each core are for the distribution of ^{137}Cs (units = mBq cm^{-2}) within the sediment core. Distributions of ^{137}Cs in the sediment profiles are plotted in detail with activity in units and standard errors on other individual figures to follow.

present in surface sediments is commonly used as an indicator of recent organic sedimentation to the benthos, e.g. Fielding et al. (1988), Cooper et al. (2002), Pirtle-Levy et al. (2009), Cooper et al., 2012; and Cooper et al., (2015). We compared these indicators of biologically-related sedimentation with the physically based indications of sedimentation from radionuclide distributions.

2. Methods

Sediment cores were collected using a HAPS benthic corer (33 cores), 133 cm^2 (Kanneworff and Nicolaisen, 1973), or a Benthos gravity 7-cm diameter corer (Teledyne Benthos, North Falmouth, Massachusetts; 7 cores, primarily on Hanna Shoal). Samples were collected during the RUSALCA program in September 2009 and September 2012 (Crane and Ostrovskiy, 2015) and the COMIDA CAB and Hanna Shoal Ecosystem Projects in August 2009, and August 2012 (Dunton et al., 2014; Dunton, 2015). Data from a single HAPS core, collected from a depth of 400 m on the Bering Sea slope in June 2007, are also provided here to show a comparison from south of Bering Strait. HAPS cores were sectioned in 1-cm segments to a depth of 4 cm, then every 2 cm below that depth. Gravity cores were sectioned every 2 cm beginning at the surface for all increments.

These sectioning intervals were selected because the sediments from the 40 cores that were collected were sealed in 90 cm^3 aluminum cans with standardized geometries at sea. Given the HAPS corer or gravity corer diameters, 1–2 cm increments were the maximum resolution that were possible to obtain and still completely fill the 90 cm^3 aluminum cans with standardized geometries that were used. The samples were returned to Chesapeake Biological Laboratory for direct gamma spectroscopy using a Canberra GR4020/S reverse electrode closed-end coaxial detector with low background shielding (Nuclear Lead Co., Oak Ridge, Tennessee). Corrections for efficiency, peak shape and calibrations for all samples were made prior to counting with a mixed gamma standard (Eckert & Zielgler Analytics, Atlanta, Georgia) traceable to the National Institute for Standards and Technology. Background corrections and a control sample (a spiked clay sample containing a known activity of ^{137}Cs in the same geometry as the samples) was analyzed for 10 min prior to counting each sample to verify detector performance and assess any long-term drift. Data for ^{137}Cs inventories are reported on an area (per cm^2) basis, because deposition of this radionuclide was generally on an areal basis based upon bomb fallout, using the 661.5 KeV peak on the gamma spectrum although we also determined radionuclide activity on a gram dry weight basis. Sediments were counted over several days (160,000–200,000 s) and then dried at 60 °C for several additional days.

^{210}Pb activity data are reported on a gram dry weight basis, because the distribution of this radionuclide is controlled by sediment characteristics in addition to areal deposition. ^{210}Pb activity was detected using the 46.5 KeV gamma decay peak. Six cores collected in 2009 were not assayed for ^{210}Pb, so ^{210}Pb data are available for 34 cores rather

Table 1
Core collection coordinates, dates of collection and maximum ^{137}Cs activity.

Cruise	Station Name	Latitude	Longitude	Collection date (M/DD/YY)	Maximum radiocesium activity (mBq cm^{-2})	Depth of radiocesium maximum (cm)	Maximum radiocesium activity at secondary peak (mBq cm^{-2})	Radiocesium activity at secondary peak relative to largest peak (percent)	Category or Comments
COMIDA09	UTX29–6	70.3451	−165.4504	7/24/09	1.65	9	1.32	80%	Ambiguous, but interpreted to be bioturbation dominated; similar deposition throughout core
COMIDA09	CBL3–03	69.8291	−165.4996	7/28/09	1.79	3.5	–	–	Single peak
COMIDA09	UTX26–12	70.6972	−165.4406	7/30/09	1.80	13	–	–	No distinct secondary peak; bioturbation dominated
COMIDA09	UTX19–15	71.0182	−164.2547	7/31/09	1.70	7	1.15	68%	Ambiguous, but interpreted to be bioturbation dominated
COMIDA09	UTX18–26	71.0774	−162.5584	8/4/09	2.00	5	1.59	79%	Sedimentation dominated
COMIDA09	UTX17–22	71.2721	−167.0144	8/5/09	2.14	9	1.74	81%	Sedimentation dominated
COMIDA09	UTX21–20	71.0773	−166.1785	8/6/09	1.96	9	1.52	78%	Sedimentation dominated
COMIDA09	CBL20–44	72.4040	−164.9580	8/8/09	1.64	3.5	1.29	79%	Sedimentation dominated
COMIDA09	CBL19–45	72.2824	−163.2889	8/10/09	1.45	5	1.31	90%	Bioturbation dominated
COMIDA09	CBL8–21	71.4847	−167.7817	8/11/09	1.44	3.5	1.36	94%	Ambiguous; interpreted to be sedimentation dominated due to lower activity at surface and at base of core
COMIDA09	CBL15–47	71.7274	−160.7183	8/11/09	1.44	5	1.40	97%	Bioturbation dominated
COMIDA09	UTX13–23	71.3871	−166.2765	8/5/09	1.70	2.5	1.59	94%	Bioturbation dominated
COMIDA09	UTX8–40	71.7254	−163.4562	8/17/09	1.40	5	0.74	53%	Sedimentation dominated
COMIDA09	CBL12–29	70.9085	−160.7408	8/3/09	2.24	9	2.23	99%	Bioturbation dominated
HLY1201	H4–25	72.5372	−162.2482	8/17/12	0.96	1	0.88	92%	Highest deposition near surface
HLY1201	H1–37	71.6518	−162.6327	8/19/12	1.03	3	0.86	83%	Deposition at surface
HLY1201	H19–38	71.7129	−161.5516	8/19/12	1.36	15	0.95	70%	Bioturbation dominated
HLY1201	H21–9	72.5200	−164.7271	8/14/12	1.30	5	0.97	75%	Sedimentation dominated
HLY1201	H20–46	72.1524	−159.9490	8/20/12	0.68	0.5	–	–	Deposition at surface
HLY1201	H32–52	71.7817	−158.9866	8/21/12	0.56	3	–	–	Deposition at surface
HLY1201	H30–11	72.7411	−163.6727	8/12/12	1.12	5	1.08	96%	Sedimentation dominates
HLY1201	H6–19	72.164	−163.603	8/6/12	0.90	11	0.59	66%	Low deposition
Rusalca09	LS1–139	69.8300	+178.0064	9/8/09	2.07	13	–	–	Single broad peak
Rusalca09	LS3–121	70.3358	+178.3300	9/8/09	1.95	7	–	–	Single peak
Rusalca09	WN2–137	72.3345	+178.5030	9/10/09	1.80	11	–	–	Single broad peak
Rusalca09	WN3–138	72.6642	+177.6690	9/10/09	1.42	2.5	–	–	Single peak near surface
Rusalca09	WN1–136	71.6648	+179.4990	9/11/09	1.51	13	1.20	79%	Deposition concentrated at base of core
Rusalca09	HC49–180	73.3563	−175.6230	9/13/09	1.96	3.5	–	–	Single peak near surface
Rusalca09	HC60–148	71.3953	−174.7790	9/17/09	1.29	3.5	–	–	Single peak, but short core
Rusalca09	CL8–30	67.8665	−172.5530	9/26/09	2.38	17	1.95	82%	No distinct peaks
Rusalca12	CS8R	67.4312	−169.6030	9/14/12	0.90	15	0.59	66%	No distinct peaks
Rusalca12	HC2	70.9000	−175.0127	9/7/12	1.65	9	–	–	Single peak
Rusalca12	CL6R	67.4312	−169.603	9/13/12	1.19	17	1.00	84%	No distinct peaks
Rusalca12	CEN1A	70.7085	−178.2988	9/6/12	0.82	15	0.69	84%	No prominent peak, low deposition overall
Rusalca12	CL3	69.0032	−168.8938	9/12/12	0.99	9	0.72	73%	Bioturbated core
Rusalca12	CS12	67.8737	−168.3142	9/14/12	1.13	11	0.99	88%	Bioturbated core
Rusalca12	HC18	71.6213	−175.4085	9/9/12	1.20	2.5	1.16	97%	No single peak
Rusalca12	HC22	71.7077	−174.8898	9/8/12	1.36	9	0.91	67%	Appears to center on one peak
Rusalca12	HC26	71.7878	−174.3945	9/8/12	1.59	13	0.62	39%	Complex deposition pattern
Rusalca12	CL8	67.8692	−172.5482	9/13/12	1.74	13	1.42	82%	No single peak

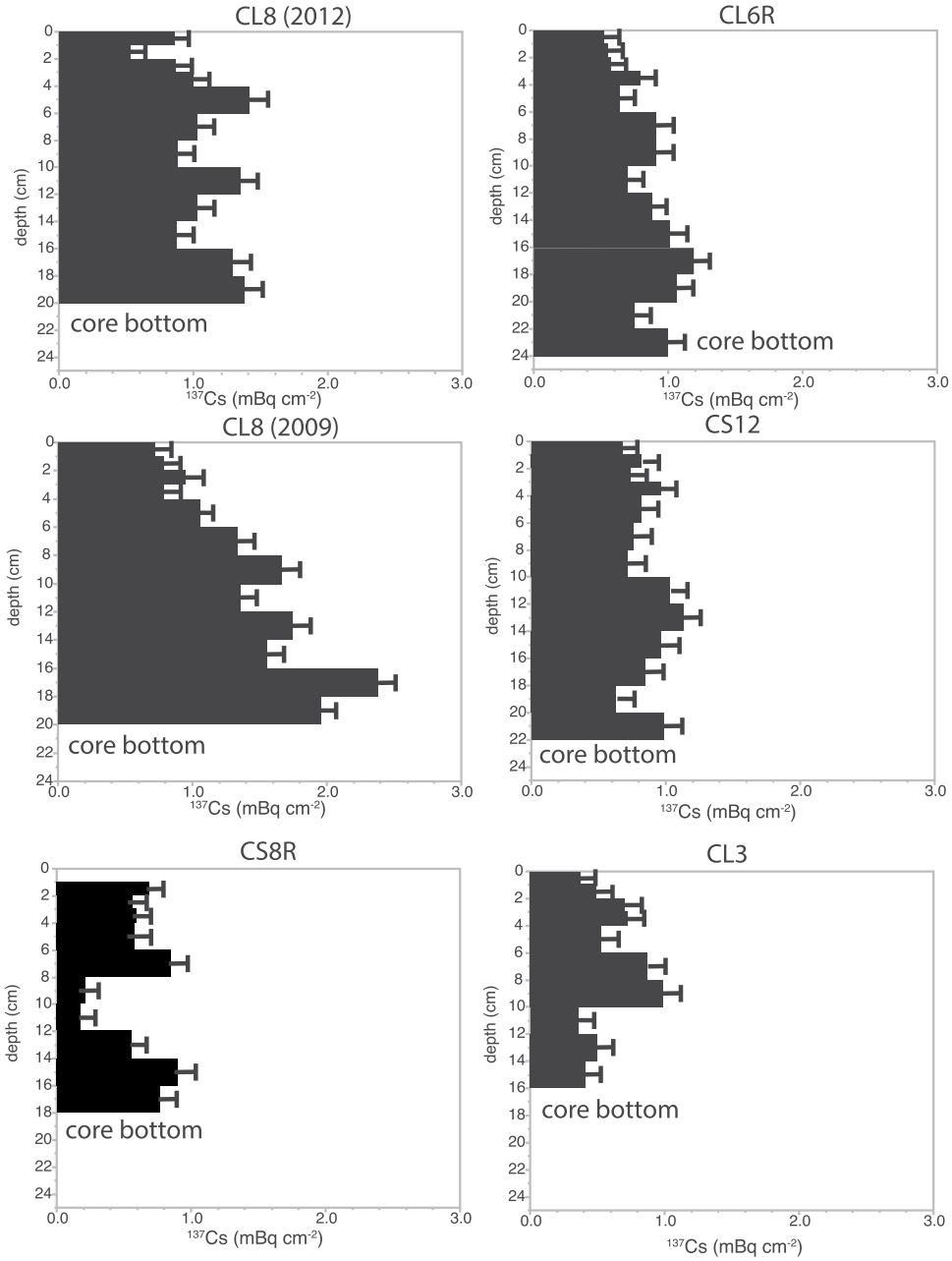

Fig. 2. Radiocesium distributions in sediment cores located in areas of high biological activity north of Bering Strait (e.g. Distributed Biological Observatory 3 hotspot), which are categorized as being most influenced by bioturbation. These cores have no single prominent ^{137}Cs maxima, but rather an even distribution of radiocesium throughout the sediment core due to benthic biological activity.

than the 40 for which ^{137}Cs data are available. Prior to drying the sediments, a self-absorption correction for ^{210}Pb (Cutshall et al., 1983) was determined by counting each sediment sample for 10 min in the presence of a sealed ^{210}Pb source with a known radioactivity (20 kBq, decay corrected from January 1, 2007) relative to activity associated with the same source placed upon an empty aluminum can. This protocol corrects for differences in water content, grain size and porosity in each core increment that affect detector efficiency. For each core increment that was assayed for ^{210}Pb, a subjective judgment was made as to the depth of the mixed layer at the surface, below which logarithmic declines in ^{210}Pb could be related to the sediment depth. The slope of this relationship was divided by the appropriate activity coefficient (for activity plotted logarithmically, -0.01352 year^{-1}). A second subjective judgment was made at the base of each core as to at what depth ^{210}Pb activity was no longer declining. The mean of all activities below that depth was used as the supported activity of ^{210}Pb.

All activities for both ^{137}Cs and ^{210}Pb are reported relative to the date of collection. Given the comparatively small range of sampling dates on the Chukchi shelf relative to half-life, we assume that differences in collection dates over the two separate years of the study (2009 and 2013) do not introduce any significant differences to interpretations that would be reached if all sampling were corrected to a common date. All raw data for ^{210}Pb and counting errors for each sediment increment are available as archived data at: https://data.nodc.noaa.gov/cgi-bin/iso?id=gov.noaa.nodc:0123220.

The grain size, TOC, C/N, and sediment chlorophyll data used have been in part reported previously, e.g. Cooper et al. (2015) or are available in public data archives (Grebmeier and Cooper, 2014, 2016). Briefly we summarize the methods used. Sediments were collected from the top of a 0.1 m^2 van Veen grab from a trap door that was opened

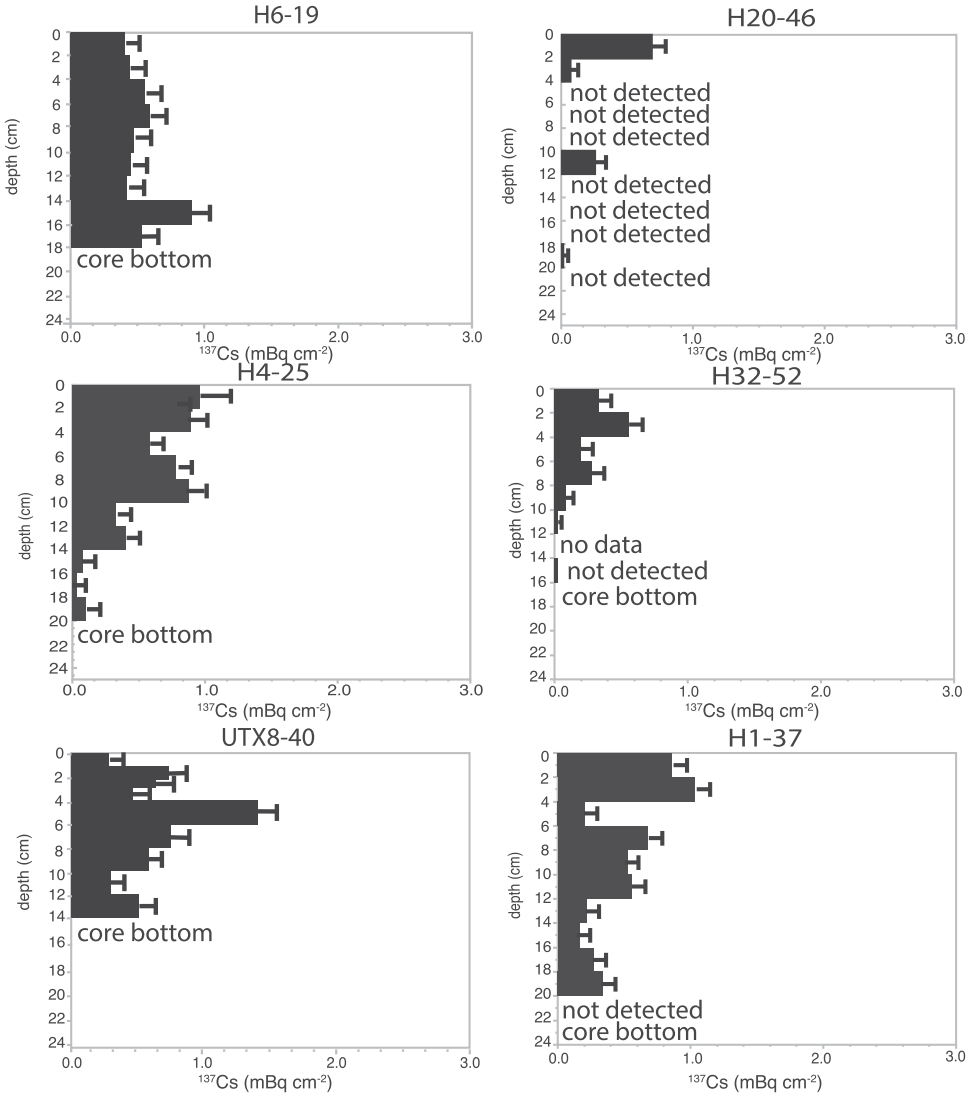

Fig. 3. Radiocesium distributions in sediment cores collected from Hanna Shoal (water depth < 45 m) that show relatively low deposition and shallow maxima. A hyphen following the station name corresponds to the station number for the 2009 and 2013 cruises that were supported through the COMIDA programs (Dunton et al., 2014, 2017).

prior to opening the grab to minimize mixing of surface sediments. Sediment chlorophyll was determined shipboard using 1 cm^3 surface sediment aliquots that were incubated with 90% acetone for 12 h at 4 °C and then measured using a Turner Designs 10 AU field fluorometer calibrated with chlorophyll standards obtained from the manufacturer (Cooper et al., 2002). Other sediment samples were returned frozen to the laboratory and the proportions of sediment grain sizes were determined by wet and dry sieving, using standard geological sieves (0–5 phi sizes). TOC and C/N ratios were determined on sediments that were acidified with 2 mL of 1 N hydrochloric and dried at 105 °C overnight to obtain carbonate-free sediments, followed by homogenization. The TOC content and the C/N ratios were determined using a Costech Model ECS 4010 elemental analyzer that was linked to a ThermoFisher Delta Plus stable isotope mass spectrometer.

3. Results

For most of these 40 cores, ^{137}Cs activity was still detected at the bottom of cores recovered, so total inventories are larger than the integrated sums of activity data that are available. Nevertheless, we assume that much of the total inventory was recovered, based upon low or near detectable activities at the base of each core. Depth profiles of radiocesium activity vary considerably among regions across the Chukchi Shelf (Fig. 1), and can be separated into different categories, albeit with some overlap. Some cores have prominent sub-surface radiocesium peaks, some do not and appear as well-mixed profiles due to bioturbation. In other cases, current flow is sufficient to erode away fine surface material such as clay minerals associated with radiocesium or alternately, it can accumulate to relatively high activities where there is little apparent current motion. Because current flow, bioturbation, and sedimentation vary widely on the Chukchi Shelf, it is convenient to categorize sedimentation and bioturbation driven core types primarily on a geographical basis. We divided the samples as follows and present the associated results: 1. Samples collected to the north of Bering Strait in an area with high biological productivity and bioturbation of sediments; 2. On the Northeast Chukchi Shelf, from water shallower than 45 m, primarily on the undersea Hanna Shoal where bottom water currents reduce sedimentation; 3. On the Northeast Chukchi Shelf in waters deeper than 45 m, where sedimentation appears to be at least as important as bioturbation; 4. In the remaining cores from the northeast Chukchi Shelf (water depth also > 45 m), where bioturbation appeared to be at least as important as sedimentation; 5. In presumably high current areas in and near Herald Canyon on the Northwest Chukchi Shelf; and 6. In Long Strait and adjoining areas of the East Siberian Sea. We summarize the characteristics of each core collected, including location, date of collection,

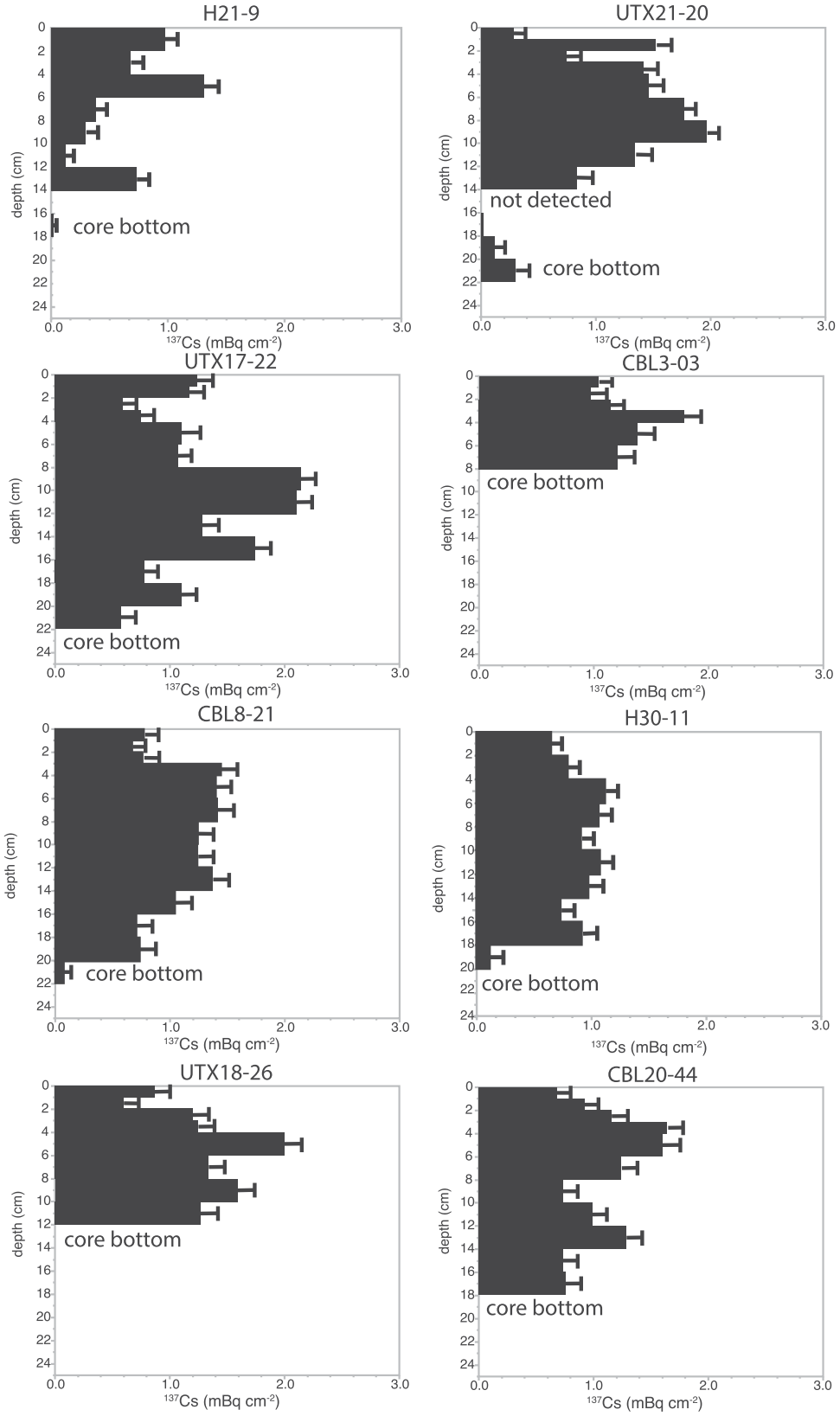

Fig. 4. Radiocesium distributions in sediment cores from the northeast Chukchi Sea. These cores are bioturbated, but in general have identifiable ^{137}Cs maxima, suggesting lower degrees of bioturbation. A hyphen following the station name corresponds to the station number for the 2009 and 2013 cruises that were supported through the COMIDA programs (Dunton et al., 2014, 2017).

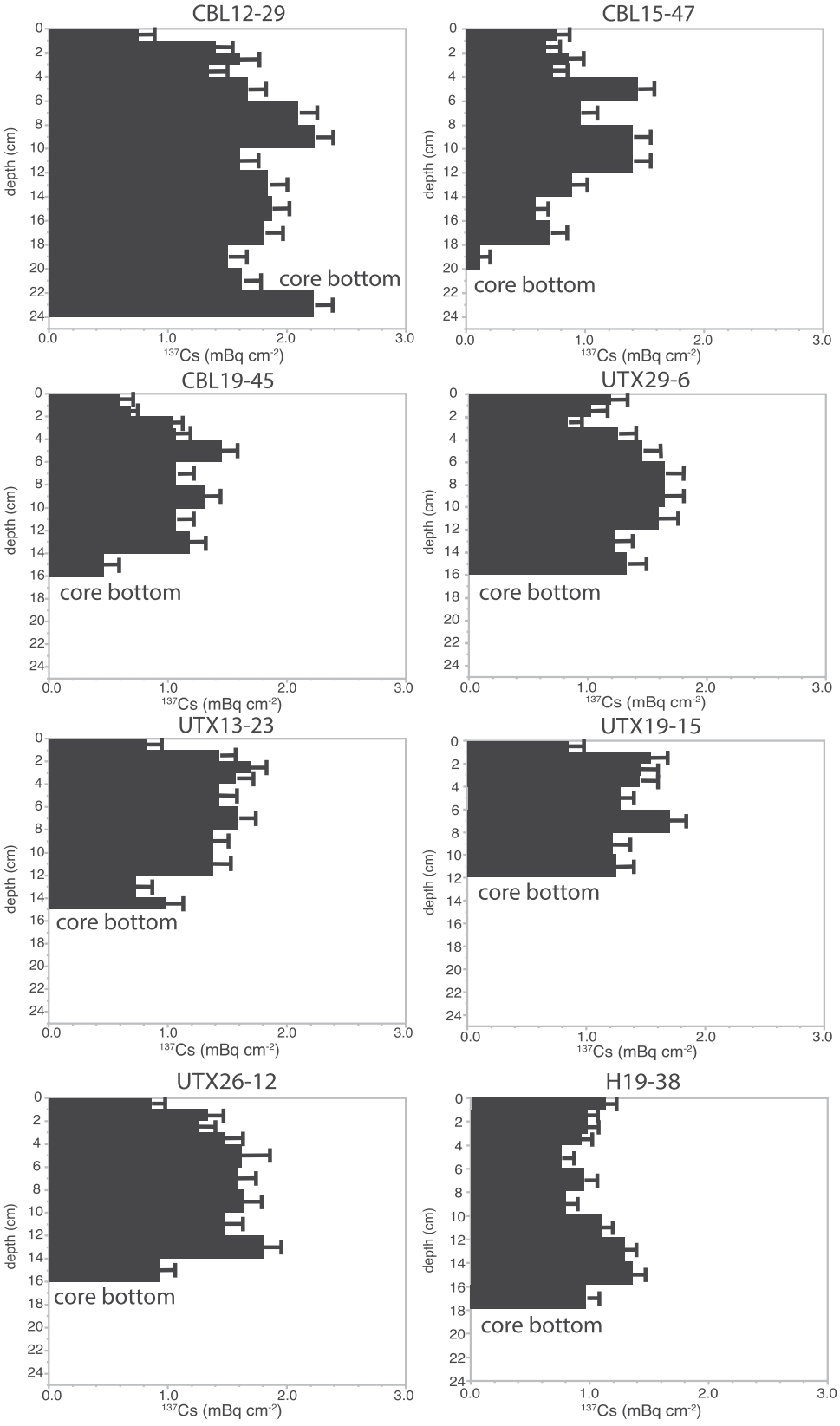

Fig. 5. Radiocesium distributions in sediment cores collected from the periphery of Hanna Shoal, where total inventories were higher than the cores collected from the Shoal and activity maxima were deeper, but radiocesium was well-mixed vertically with no prominent subsurface peak, implying that bioturbation was a more dominant mixing agent, as in the biologically productive DBO3 cores (Fig. 2). A hyphen following the station name corresponds to the station number for the 2009 and 2013 cruises that were supported through the COMIDA program (Dunton et al., 2014, 2017).

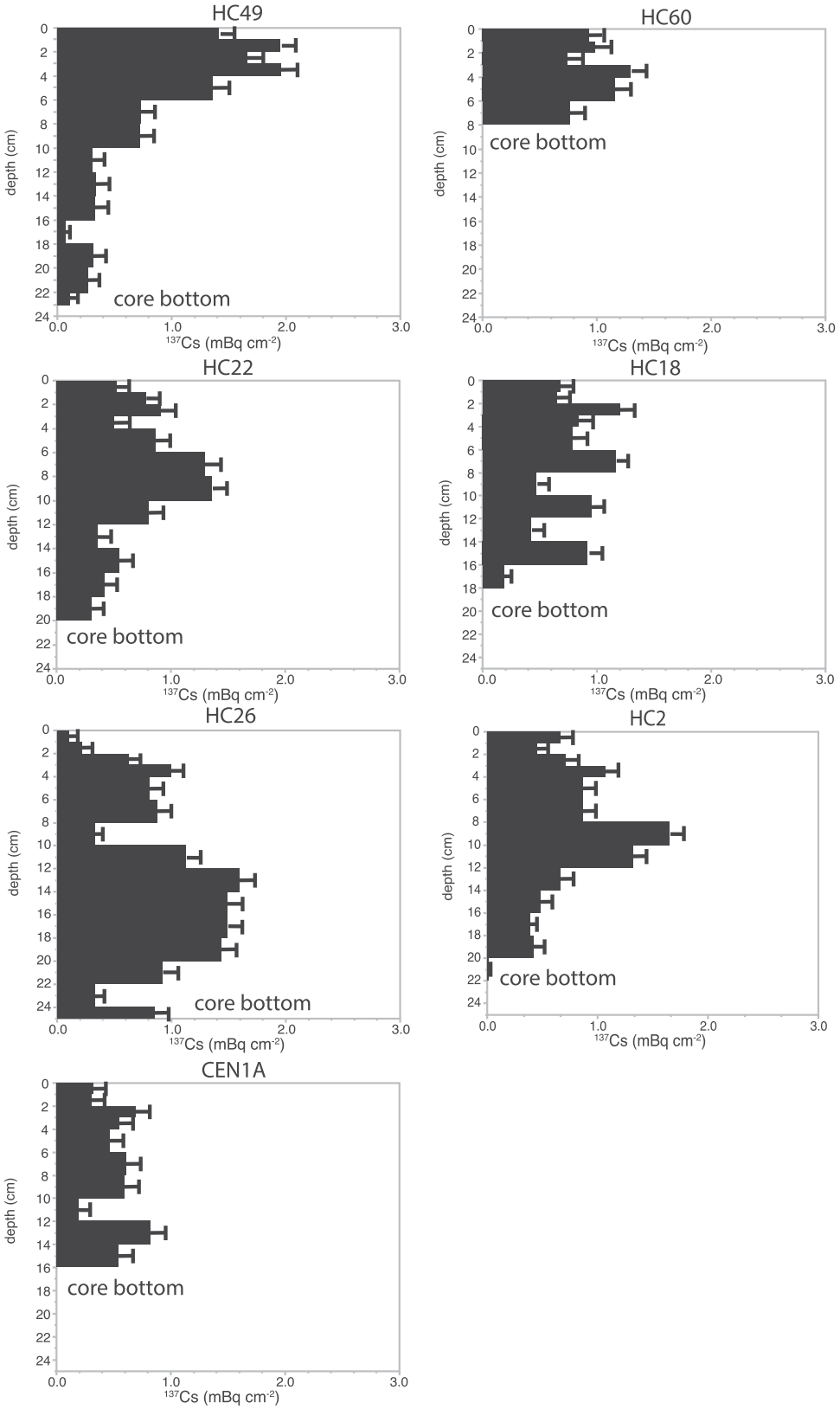

Fig. 6. Radiocesium distributions in sediment cores collected from high current regions within Herald Canyon, and south of Wrangel Island. Some of these cores show radiocesium burdens close to the sediment surface, implying erosional current flow.

maximum activity detected, and the presence of any secondary maxima in Table 1. Using criteria such as the presence of secondary maxima, we also provisionally categorized many of the cores as being dominated by bioturbation processes or sedimentation, while recognizing that both processes are important throughout the Chukchi Shelf.

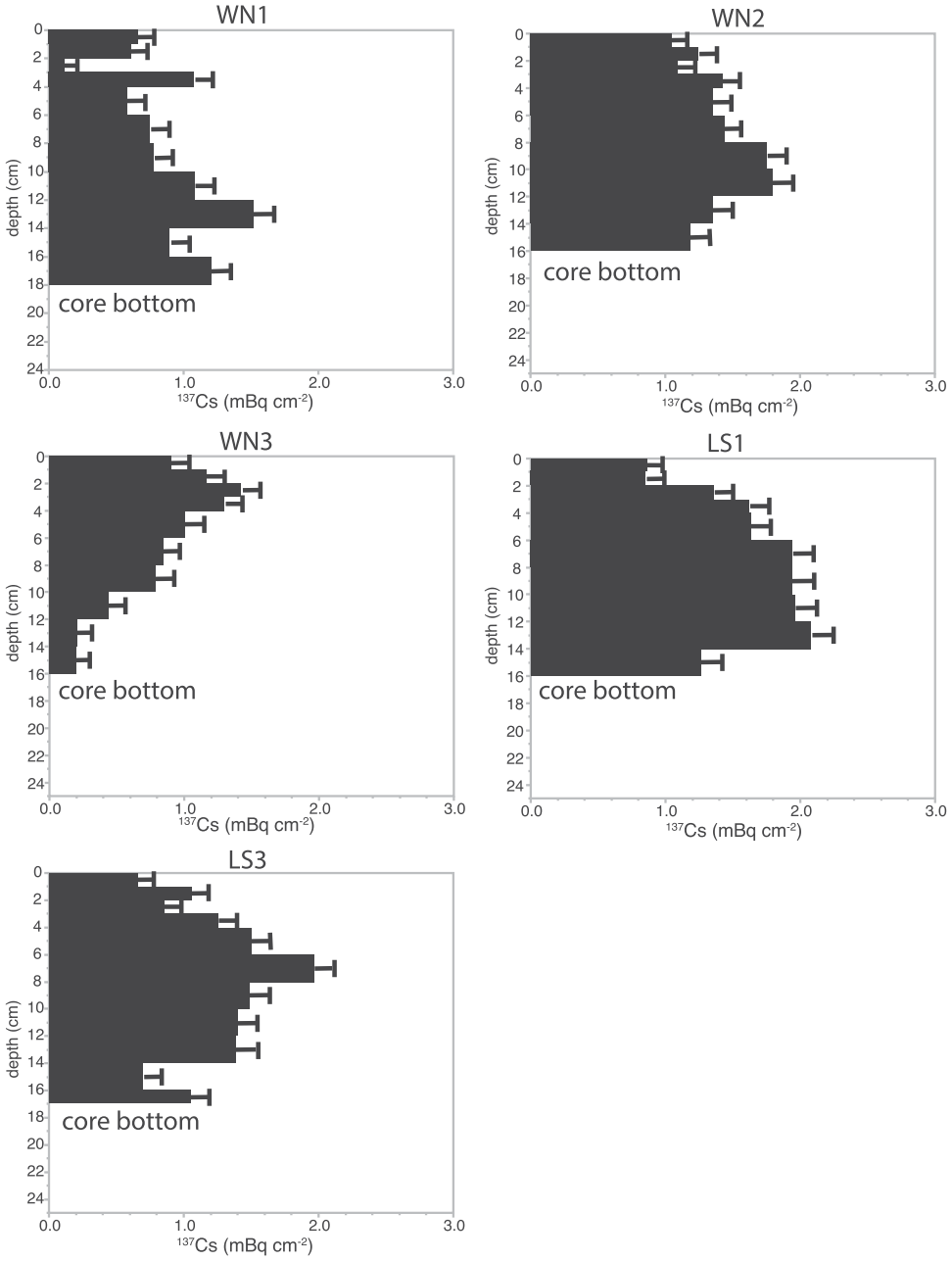

Fig. 7. Radiocesium distributions in sediment cores collected north of Wrangel Island and in Long Strait (Fig. 6). Higher maximum activities (~2 mBq cm^{-2}) imply quiescent conditions and settlement of fine particles.

3.1. Bioturbation Dominates, Distributed Biological Observatory 3

In the biologically productive area that constitutes the Distributed Biological Observatory (DBO, reviewed in Moore and Grebmeier, 2017), which is part of long-term sampling immediately north of Bering Strait (DBO Sampling Area 3, hereafter DBO3; Fig. 2) radiocesium profiles show evidence of significant bioturbation because there is, in most cases, no identifiable, distinct maximum activity that preserves the 1963–1964 bomb fallout maximum. This maximum would be characterized by lower activities above (meaning more recent deposition of less contaminated sediments) and lower activities below a peak (meaning older deposited sediments prior to the bomb fallout maximum). Maximum activities were detected at depth within each core, but activities were moderate (i.e. not among the highest observed during the study) and vary within a narrow range (mean maximum activity 1.17 mBq cm^{-2} ± 0.22 SD, n = 6); activities within the surface sediments that were assayed were lower, but also varied within a narrow range (mean = 0.64 mBq cm^{-2} ± 0.17 SD). Activity maxima at depth were 1.3–2.6 times higher than at the surface. These cores do not have activities declining to minima at the bottom of the cores. This characteristic, the relatively low total activities compared to cores collected from other regions, the narrow range of variation, and the modest differences between the surface and the depths where maximum activities were detected indicate that in most cases, radiocesium has been mixed to depths of 20 cm or more by the abundant benthic biological community present in this area (Grebmeier et al., 2015).

3.2. Hydrographic influences at Hanna Shoal

A variation from these high bioturbation core patterns was observed for the northeast Chukchi Shelf cores collected from the shallowest locations (< 45 m) sampled on Hanna Shoal (Fig. 3), where total

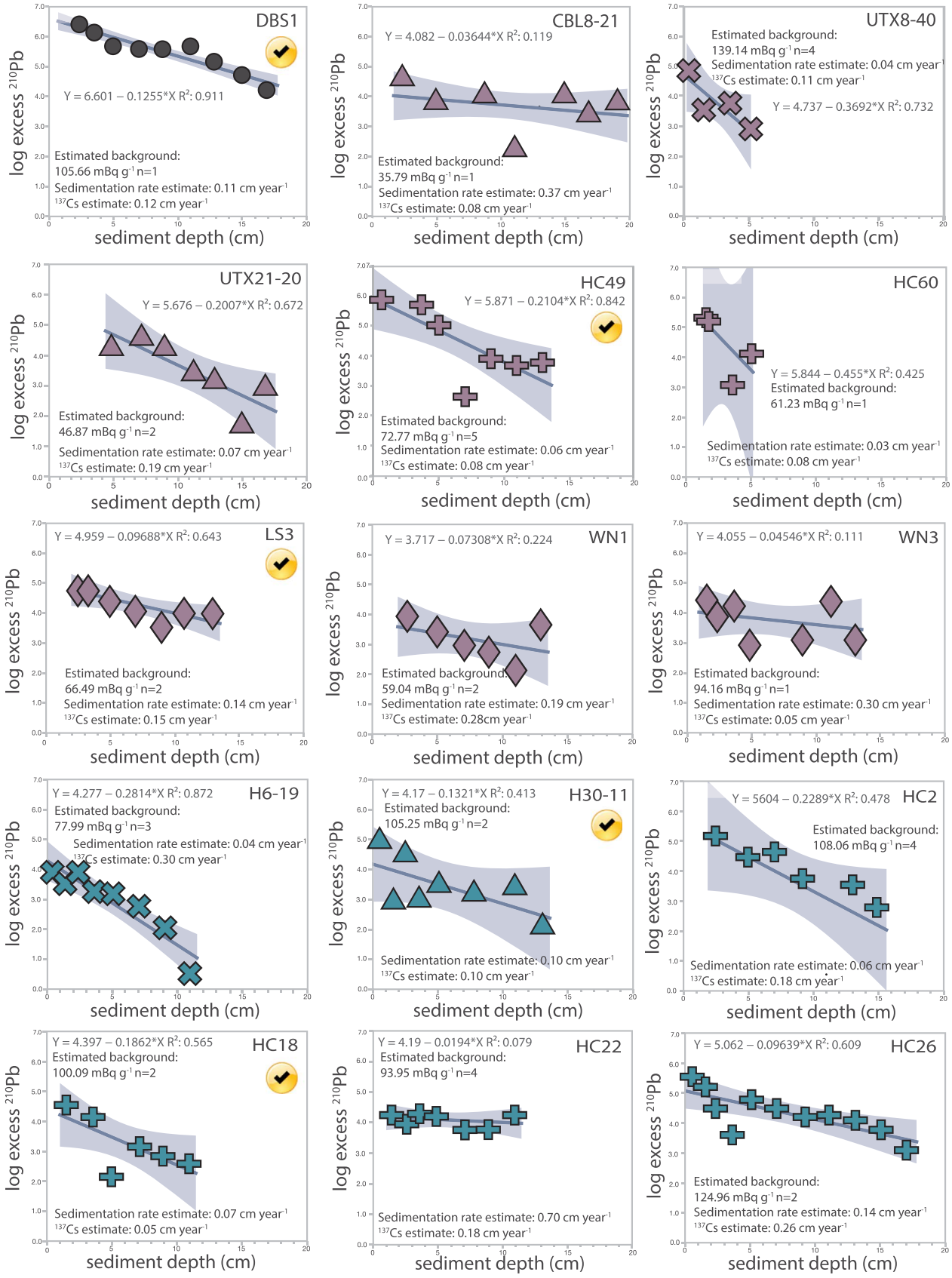

(caption on next page)

Fig. 8. Log of ^{210}Pb excess regressions relative to sediment depth for 1 deep (400 m) core collected in the northern Bering Sea [DBS1 and for 14 cores (of 34 counted)] where there was a steady decline in excess ^{210}Pb (above background or supported), moving down the sediment core. Symbols and colors are same as for Fig. 1. Background or supported ^{210}Pb provided for each core is based upon activities at the base of the core (number of activities averaged is given as n =). Sedimentation estimates from ^{210}Pb were calculated from the activity coefficient for ^{210}Pb (-0.01352 year^{-1}) divided by slope of the line relating log excess ^{210}Pb to sediment depth (cm). The yellow checked circles indicate cores where there was good agreement (difference of < 0.02 cm year^{-1}) between sedimentation rate estimates provided by both ^{210}Pb and ^{137}Cs; both sedimentation rates are given. Some data in well-mixed surface sediments were excluded and are not plotted here (see Section 2). A hyphen following the station name corresponds to the station number for the 2009 and 2013 cruises that were supported through the COMIDA programs (Dunton et al., 2014, 2017).

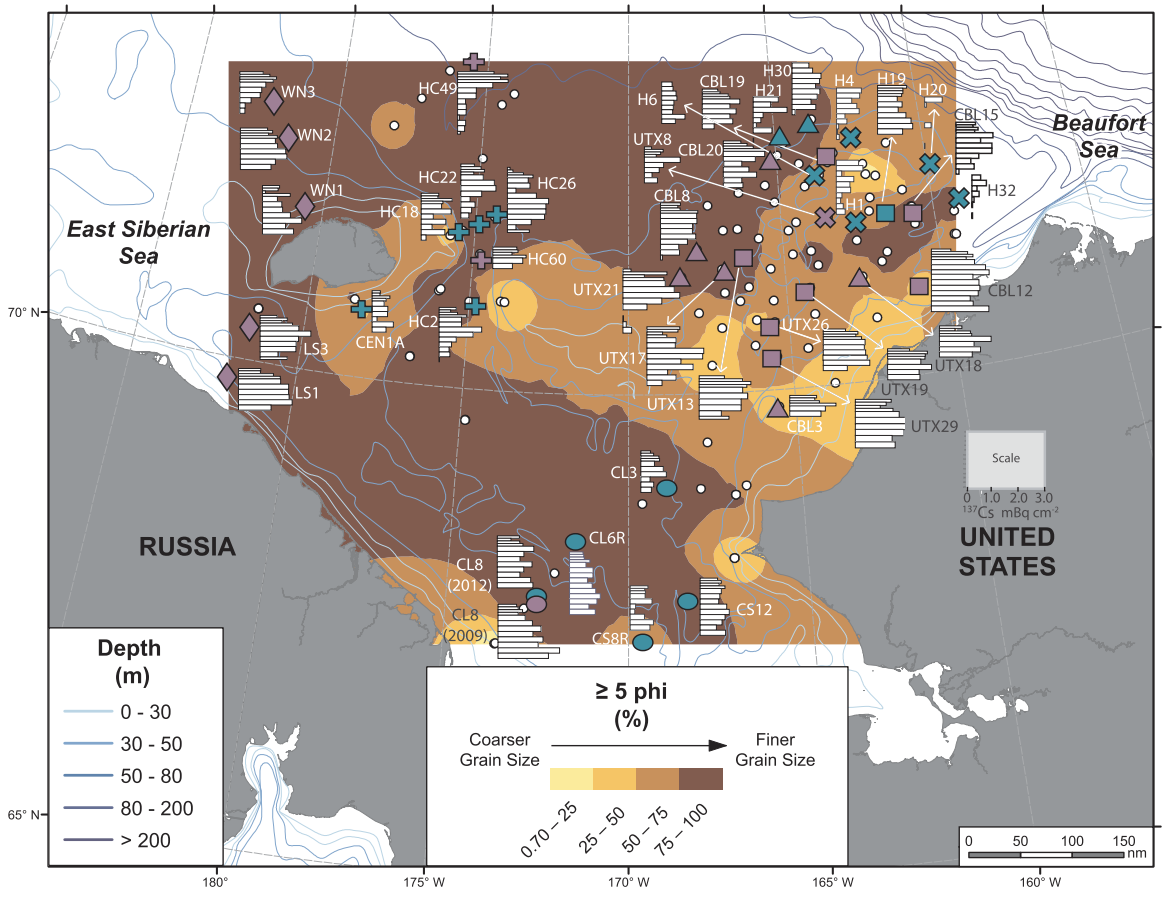

Fig. 9. Distribution of fine-grained surface sediments on the Chukchi shelf using the proportion (weight percent) of sediments passing through a ≥5 phi sieve (~30 μm). Miniaturized profiles are for the distribution of ^{137}Cs (units = mBq cm^{-2}) within the sediment core. Distributions of ^{137}Cs in the sediment profiles are plotted in detail with activity in units and standard errors on other individual figures. Symbol key and coloring scheme for symbols is the same as in Fig. 1.

deposition of the radionuclide over the whole sediment core was generally lower, and radiocesium maxima (mean = 0.88 mBq cm^{-2} ± 0.36; n = 6) were at shallower depths (mean = 4.7 cm), suggesting higher currents, lower deposition, and moderate bioturbation. The cores collected at stations H6-19 and H4-25 may be considered exceptions as the sediment depth of the radiocesium activity maximum was at 15 cm and 9 cm, respectively, but otherwise no activity maximum in this group was observed deeper than 5 cm in the sediments. Due to the sediment structure on Hanna Shoal, which includes gravel in the shallowest portions of the shoal, not all coring attempts were successful.

3.3. Cores from Northeast Chukchi Sea Where Sedimentation > Bioturbation

On the northeast Chukchi Shelf in waters deeper than the cores from Hanna Shoal (> 45 m), sedimentation sometimes dominates over bioturbation, leading to many cores with mid-depth maxima of ^{137}Cs (Fig. 4), as well as minima at the bottom of the recovered cores. In other cases, however, bioturbation appeared to be more important, and core profiles were well-mixed without prominent individual subsurface maxima. While recognizing that the distinction between the two categories of cores (bioturbation versus sedimentation dominated) can be ambiguous, we used the presence of apparent secondary maxima to help categorize the dominance of the two processes (Table 1). Where the activity of ^{137}Cs at a separate, secondary maximum was 90% or more of the activity at the primary maximum (see Table 1), we assumed a well-mixed core dominated by bioturbation. Where separate secondary maxima were less than 90% of the activity present at the depth of maximum activity, we categorized the core as retaining characteristics of the original sedimentation. In several cores from the northeast Chukchi Shelf, specifically UTX29-6. UTX19-15, and CBL8-21, we reached different conclusions than suggested by this criterion that assessed the difference between secondary and primary peaks in radiocesium activity. For core UTX 29-6, the secondary peak was 80% of the activity present in the primary maximum, but relatively even distribution throughout the core (Fig. 5) suggested that bioturbation dominated. For core UTX19-15, the secondary ^{137}Cs peak was 68% of the maximum activity, but we also interpreted the core as being bioturbation dominated because of relatively even distribution of the radionuclide within the core. By contrast, we interpreted core CBL8-21 (secondary peak was 94% of the maximum activity observed in the core) to be sedimentation dominated because of lower radiocesium burdens at the surface and base of core. In general, for the northeast

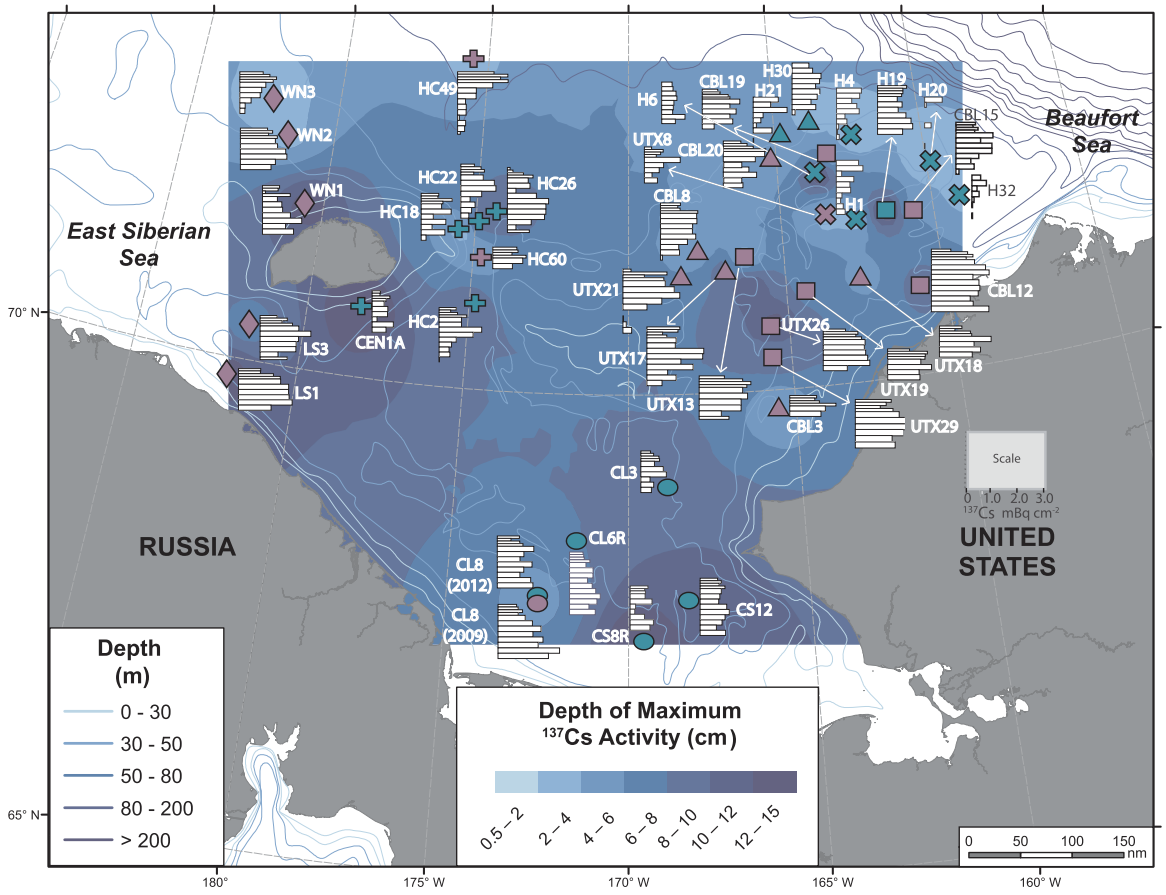

Fig. 10. Depth (in cm) of where the maximum in radiocesium activity was observed in cores collected in 2009 and 2012. The miniaturized, equally scaled profiles shown for each core are for the distribution of ^{137}Cs (units = mBq cm^{-2}) within the sediment core, which are plotted with activity in units and standard errors are on other individual figures. Symbol key and coloring scheme for symbols is the same as in Fig. 1.

Chukchi Shelf cores where sedimentation appeared to be more important than bioturbation, collected from > 45 m depth, surface sediment ^{137}Cs activities were again relatively lower at the surface (mean = 0.81 mBq cm^{-2} ± 0.29 SD; n = 8) than maximum activities observed in the cores (mean = 1.67 mBq cm^{-2} ± 0.37 SD). Maximum activities within each core were 1.3–7.0 times higher than at the surface, implying initial burial of radiocesium on clay particles during the bomb fallout era of the 1960s, followed by continued deposition of clay particles with lower radiocesium burdens, and less sediment mixing than observed in more productive areas of the shelf that have higher bioturbation (discussed in a previous section). Low re-distribution of radiocesium by boundary currents and other sea floor processes following that initial sedimentation are also implied by these core profiles.

3.4. Bioturbation dominated cores from the Northeast Chukchi shelf

In addition to the two cores discussed in the previous section, UTX29–6 and UTX19-15, we categorized six other cores from the northeast Chukchi Shelf as also being dominated by bioturbation (Fig. 5). These eight cores had apparent total inventories that were higher than the cores collected from Hanna Shoal (mean maximum activity within each core = 1.67 mBq cm^{-2} ± 0.28 SD; n = 8) and activity maxima intervals were deeper in the sediments (mean = 8 cm ± 4 SD; Fig. 5), In general in these cores, radiocesium was well-mixed vertically with no single prominent subsurface peak, implying that bioturbation was a more dominant mixing agent, as in the biologically productive DBO3 cores (Fig. 2). Although biological productivity is not as prominent on the flank of Hanna Shoal as it is in the DBO3 region (Grebmeier et al., 2015), specific areas have been identified with biological production that reaches the seafloor, such as the feeding area for walruses that is used in the late summer as seasonal sea ice declines (Jay et al., 2012; Beatty et al., 2016). These sediment profiles support the presence of significant bioturbation and associated benthic biological communities in localized areas around Hanna Shoal.

3.5. High current areas such as Herald Canyon

In areas with presumed higher current flow, such as the Herald Canyon undersea feature on the northern shelf, ^{137}Cs sediment activities tended to be high relative to other regions and core categories (mean maximum = 1.40 mBq cm^{-2} ± 0.36; n = 7). In three of the six cores (HC49, HC18 and HC60), this maximum was close to the surface, implying lower clay particle deposition, and lower sedimentation rates (Fig. 6; mean of sediment depth with maximum radiocesium activity was 3 cm ± 0.5 SD). These three cores were collected more directly in Herald Canyon (Fig. 1) than HC22 and HC26, where maxima were observed at 9 cm and 13 cm, respectively (Fig. 6), and these two cores were collected on the flank of the canyon wall (Fig. 1). HC2, which was collected upstream of the canyon (Fig. 1) also had a deeply buried radiocesium peak at 9 cm. These profiles imply that the influence of current flow within Herald Canyon is localized. Low overall activities in a core collected south of Wrangel Island (CEN1A) imply high current flow and low radiocesium deposition. Some bioturbation however resulted in deep burial in this core of the radiocesium peak (15 cm).

3.6. East Siberian Sea and Long Strait

In five cores collected north of Wrangel Island in the East Siberian

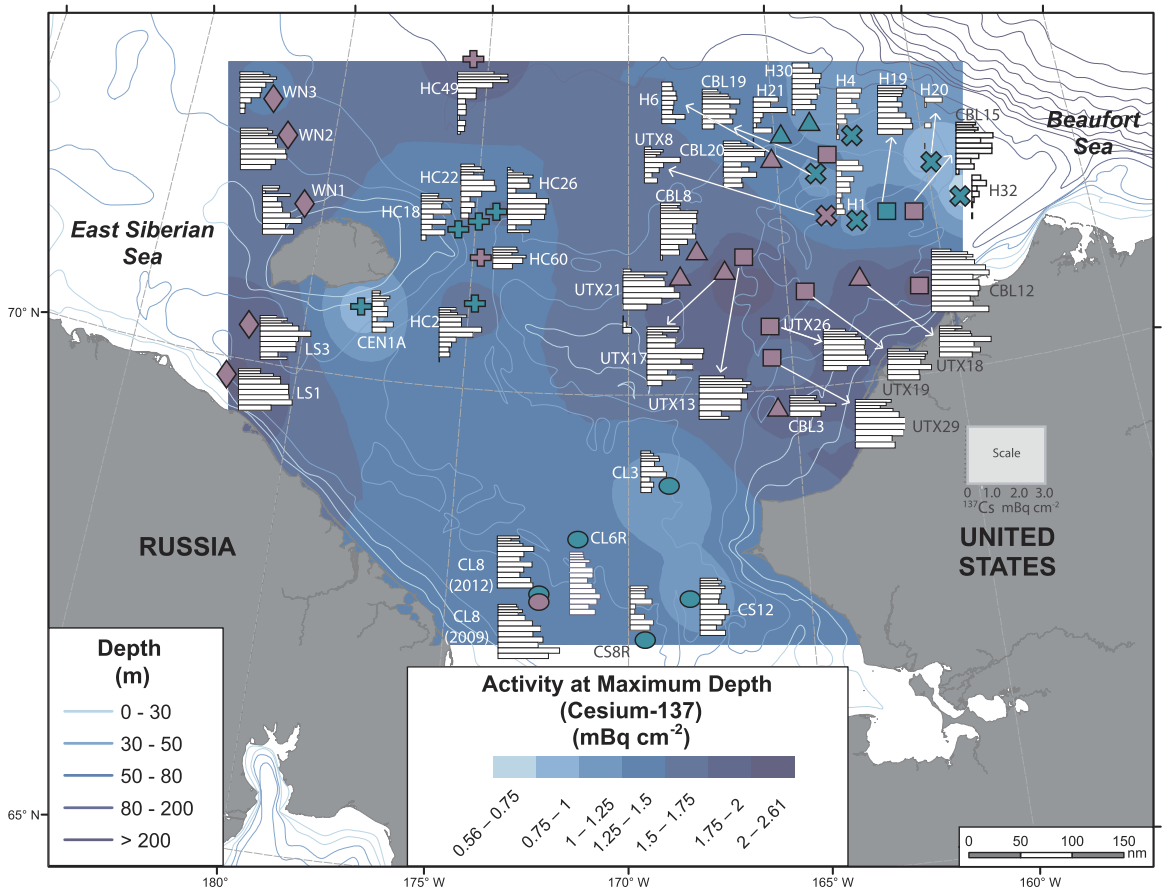

Fig. 11. Radiocesium activity at the depth where maximum activity was observed. Data are corrected to core collection date in 2009 or 2013. The miniaturized, equally-scaled profiles shown for each core are for the distribution of ^{137}Cs (units = mBq cm^{-2}) within the sediment core, which are plotted with activity in units and standard errors are on other individual figures. Symbol key and coloring scheme for symbols is the same as in Fig. 1.

Sea, and in Long Strait between Wrangel Island and the Russian mainland in 2009, lower current flow, and dominance of bioturbation over sedimentation was implied by sediment ^{137}Cs activities that remained relatively high throughout the core lengths (Fig. 7). The mean maximum activity that was observed for the core increments was 1.75 mBq cm^{-2} ± 0.28 SD; n = 5. In general, these profiles were also similar to those in areas of high biological activity to the south (Fig. 2), but maximum activities in the profiles from the East Siberian Sea and Long Strait cores were higher, up to 2 mBq cm^{-2} at specific depths, suggesting that fine particle deposition with higher ^{137}Cs burdens under quiescent currents, may have resulted in higher total inventories.

3.7. ^{210}Pb profiles

The distributions of ^{210}Pb within the 34 cores where data are available from the Chukchi Shelf reflect many of the same bioturbation and sedimentation patterns as observed for ^{137}Cs. Bioturbation limited the number of cores with steady, logarithmic declines in ^{210}Pb to only 14 of the 34 cores assayed. In addition, sedimentation rate estimates obtained for the 14 Chukchi shelf cores were consistent with sedimentation rate estimates obtained from maximum ^{137}Cs peaks in only 4 of the 14 cores (Fig. 8, checked sub-plots). We define consistent sedimentation rate estimates for the two methods as cases where the two independently estimated sedimentation rates are within 0.02 cm yr^{-1} of each other. For comparison, a single core (DBS1) was collected in deeper water (400 m) on the Bering Slope in 2007. This core had a more robust ^{210}Pb regression coefficient, and provides a more reproducible comparison with ^{137}Cs sedimentation rates (Fig. 8) as has been observed in deeper waters on the Chukchi Shelf (Pirtle-Levy et al., 2009).

4. Discussion and synthesis

The sediment characteristic patterns over the Chukchi shelf are consistent in many respects with the radiocesium profiles because of the affinity for cesium to be attached to fine clay particles. For example, grain size is coarser (lower % silt and clay fraction, i.e. < 5 phi) on Hanna Shoal and in near shore areas of the Alaska and Russian shorelines (Fig. 9). This is also reflected in many of the cores collected in the shallowest waters over Hanna Shoal, such as H6, H4, H32, and H20, where total maximum activity of radiocesium is relatively low, and maximum peaks are relatively higher in sediment cores, although core H6 is an exception with maximum activity at 15 cm (Figs. 10 and 11). High erosional water currents are implied for at least some of the sediment cores collected in locations in and near Herald Canyon, particularly HC49. Cores in Herald Canyon tended to have maximum activities closer to the sediment surface. In general, maximum activities are higher in the Herald Canyon cores than on Hanna Shoal (although not at CEN1A). These maxima are shallower in core profiles than in the biologically more productive areas such as the DBO3 “hot spot” in the southern Chukchi Sea (Figs. 1, 10, 11). The activity of radiocesium at the sediment maximum (Fig. 11) therefore can be interpreted to reflect a combination of sedimentation as well as bioturbation that diminishes the intensity of the ^{137}Cs activity maximum.

Other sediment characteristics that are physically related to grain size distributions can contribute additional insights. Prior work in the Bering, Chukchi, and East Siberian seas has shown that radiocesium activities in surface sediments are significantly correlated with fine grain sizes (≥5 phi) and TOC (Cooper et al., 1998a). Higher TOC indicates where currents slow down and fine settling of organic particles

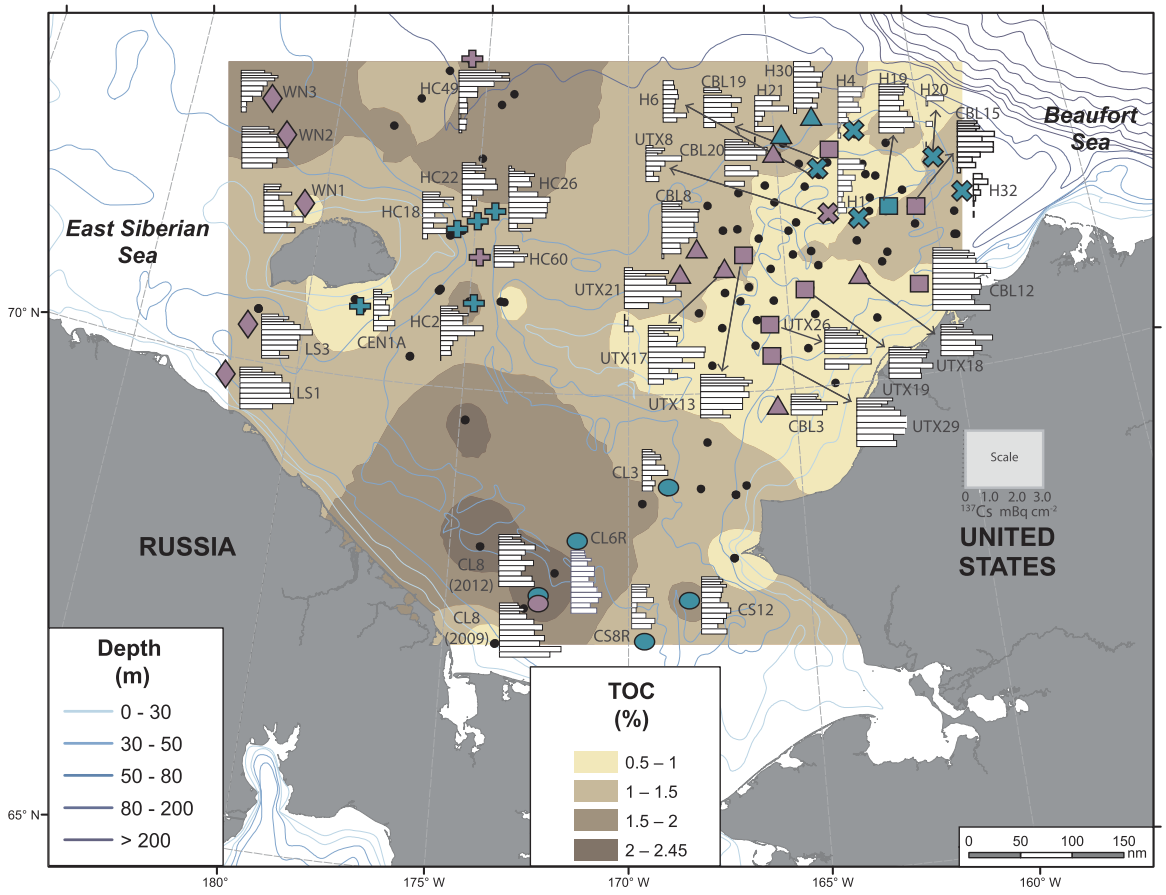

Fig. 12. Distribution of total organic carbon on the Chukchi shelf (weight percent) relative to miniaturized radiocesium profiles (units = mBq cm^{-2}) for the sediment cores reported here. Distributions of ^{137}Cs in the sediment profiles are plotted in detail with activity in units and standard errors on other individual figures. Symbol key and coloring scheme for symbols is the same as in Fig. 1.

can occur. Fine settling of organic particles is also often matched to high benthic biological activity in the Chukchi Sea (Grebmeier et al., 2015). Distributions of TOC across the Chukchi Shelf show that the highest TOC in surface sediments was found in the DBO3 benthic hot spot region in the southern Chukchi Sea and north of Wrangel Island (Fig. 12). The difference in the sediment core profiles of radiocesium between these two regions largely centers on the impacts of bioturbation, which is prominent in the DBO3 region where there is high benthic biomass (Grebmeier et al., 2015), driven by high primary production (Hill et al., this volume). North of Wrangel Island, in the East Siberian Sea, and in Long Strait, mid-depth and sub-surface maxima in radiocesium activity are apparent (Fig. 14), meaning that quiescent currents permit settling of fine particles. However, bioturbation is less significant, which is consistent with lower benthic biomass, based upon the limited data that are available from north of Wrangel Island (Grebmeier et al., 2015). The core profiles from Long Strait, where there is little direct data available on current speeds, also indicate low current speeds and differ from those collected in Herald Canyon, where higher currents are apparent, based upon the erosional profiles with radiocesium concentrated in some cores near the surface (Fig. 6).

C/N ratios in sediments reflect broadly the quality of organic matter reaching the bottom (Meyers, 1994). The distribution of C/N ratios on the Chukchi Shelf show that lower ratios associated with higher quality organic matter predominate in the DBO3 hotspot region, but are also present on Hanna Shoal and north of Wrangel Island (Fig. 13). Localized areas with terrestrial influence are present along the Alaska coast and southeast of Wrangel Island, where there are indications that Alaska Coastal Water can sometimes be directed (Pisareva et al., 2015). However, there are less obvious connections between the C/N ratios and the sedimentation patterns that we observed for radiocesium in the cores we collected. This is consistent with an extensive survey undertaken of surface sediment organic C/N ratios in relation to ^{137}Cs activities in surface sediments of the Bering, Chukchi and East Siberian seas (Cooper et al., 1998a). No significant relationship was found between those two parameters nor for any relationship between radiocesium and another biologically influenced characteristic, the stable carbon isotope composition of organic carbon in surface sediments. The lack of correlations for these indicators while grain size and TOC on fine particles are significantly correlated to radiocesium activity suggest the importance of physical processes including currents and sedimentation upon radiocesium deposition, even while biological processes such as bioturbation clearly influence vertical sedimentary distributions of the radionuclide.

One other sedimentation indicator we considered, sediment chlorophyll inventories, were highest on the Chukchi Shelf in the DBO3 hot spot region north of Bering Strait (Fig. 14), but were also surprisingly high north of Wrangel Island ($> 20\ mg\ m^{-2}$). Because this variable is an indicator of recent short-term sedimentation of organic carbon to the benthos, areas with low sediment chlorophyll inventories can also be areas with high bottom current flow such as Herald Canyon. The erosional radiocesium profiles observed in Herald Canyon, such as at stations HC22 and HC49, where radiocesium in the sediments was concentrated at the top of sediment cores or in the top half of the core, were consistent with these observations (Fig. 6).

Prior sediment core data reported from the Chukchi shelf, slope and Canada Basin (Pirtle-Levy et al., 2009) complement and help to put into context the data reported here as most of those cores were collected in

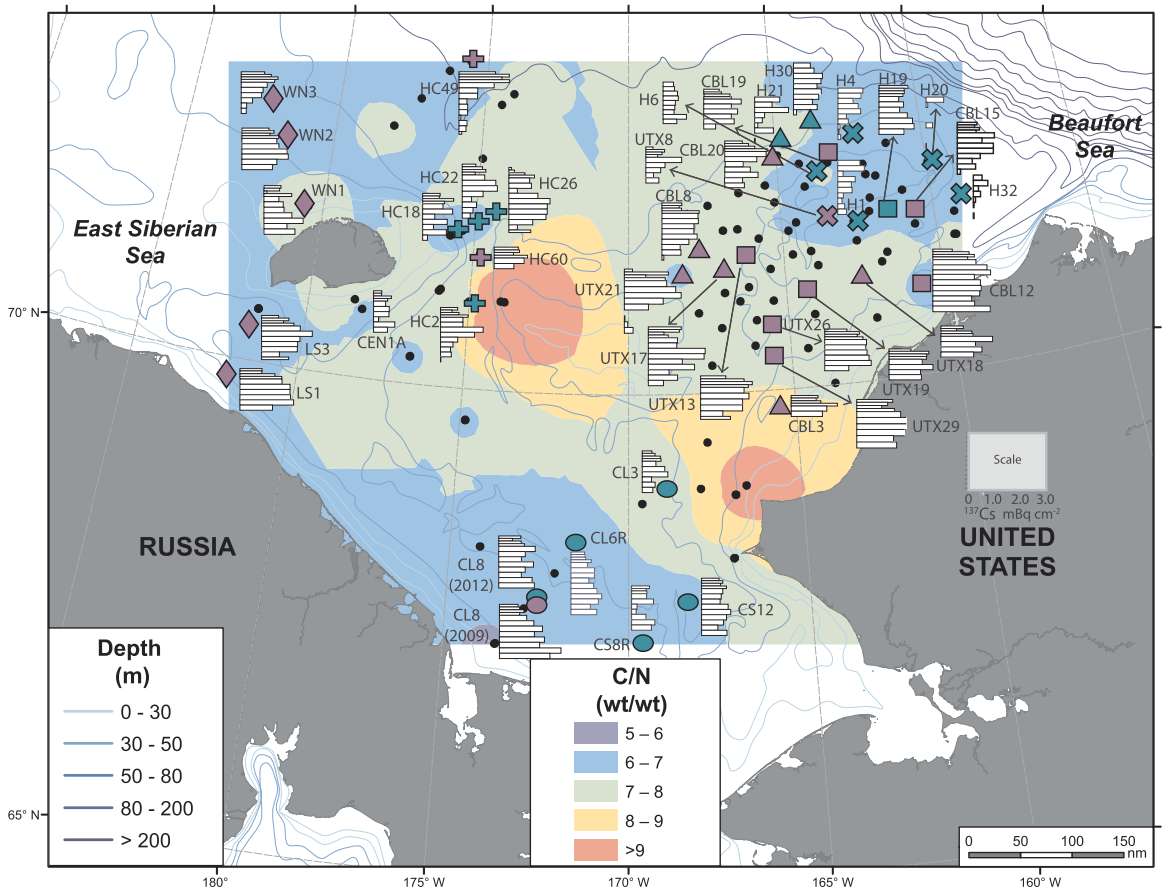

Fig. 13. Distribution of C/N ratios (weight/weight) in the organic fraction of Chukchi Shelf surface sediments relative to miniaturized radiocesium profiles for the sediment cores reported here. Distributions of ^{137}Cs in the sediment profiles are plotted in detail with activity in units and standard errors on other individual figures. Lower C/N ratios correspond to more marine organic material. Symbol key and coloring scheme for symbols is the same as in Fig. 1.

transects that extended off the continental slope into the deep Basin. Some cores were collected on the continental shelf and were similar in the depth of radiocesium penetration (~20 cm) and the well-mixed patterns we observe here. However, maximum activities observed in the continental shelf cores collected by Pirtle-Levy et al. (2009) were significantly higher (6 mBq cm^{-2} and higher) than the maxima we observed in this study (~2 mBq cm^{-2}). Given the near decade that had passed since the Pirtle-Levy et al. (2009) cores had been collected (in 2002–2004), lower activities would be expected given radioactive decay, but radiocesium appears to be declining faster than can be attributed solely to radioactive decay over its 30.2 year half-life. Measurements of ^{137}Cs in surface sediments of the Beaufort, Chukchi and East Siberian seas in 1991–1995 showed activities averaging 3.5 ± 2.3 Bq kg^{-1} dry weight (n = 145); (Cooper et al., 1998b). Converted to a dry weight basis from the per square meter inventory data provided in this study, very few surface samples in this study have even 50% of the average burden by weight present during the 1990s (mean = 1.3 ± 1.0 Bq kg^{-1} dry weight; n = 40). Pirtle-Levy et al. (2009) reported highest maximum activities in individual 2 cm core increments (~8 mBq cm^{-2}) on the continental slope at depths of 500–1000 m, probably due to transportation of clay particles containing ^{137}Cs vertically down the slope. Once in the deep water of the Canada Basin, and far enough away from the slope, radiocesium burdens decline to very low levels, but the high burdens in continental slope sediments and the significantly lower activities we report here relative to measurements made by Pirtle-Levy et al. (2009) and earlier by Cooper et al. (1998a) indicate that there is active transport of clay particles off the shelf and into slope sediments, if not into the deep basin. The incorporation of fine clay particles from continental shelf sediments into ice rafted sediments entrained in sea ice may be one possible mechanism (Cooper et al., 1998b). Other sinks for the radioisotope may be mixing deeper into the sediments below the maximum depth of the cores recovered, and loss from the sediments by dissolution from clay particles. The probable arrival of radiocesium into the Arctic through Bering Strait from the Fukushima-Daiichi nuclear power plant accident will make these determinations more difficult, but also suggests that any loss of cesium from the mostly dissolved radiocesium plume in the water column onto fine particles could be potentially detected by comparing with the radiocesium content of sediments measured on the Chukchi shelf both in the 1990s and during this study.

A sedimentation rate estimate for the Chukchi Slope using ^{210}Pb was reported by (Pirtle-Levy et al., 2009), but that study estimated sedimentation rates using both radionuclides from only one core of many collected. This sediment core, collected on the Chukchi Slope at a depth of 1496 m, resulted in two somewhat different sedimentation rate estimates (0.075 cm year^{-1} for ^{137}Cs and 0.06 cm year^{-1} for ^{210}Pb). In order to help facilitate these sedimentation rate estimate comparisons, we also present here for comparison the ^{137}Cs activity in a core collected on 17 June 2007 at 400 m depth on the Bering Sea Slope (Fig. 15). Relative to the other samples in our study, and probably due to the greater water depth of collection and lower sedimentation rates, ^{137}Cs activity is lower throughout the core (< 1 mBq cm^{-2}), and is concentrated nearer the surface. Bioturbation of radiocesium also extended no deeper than 16 cm depth for this core, so the patterns of deposition of radiocesium on the Bering Sea Slope are significantly different than observed on the Chukchi Shelf. A sedimentation rate of 0.11 cm year^{-1} was estimated for this core from ^{210}Pb distributions within the core (Fig. 8). Although it is problematic to pick an individual

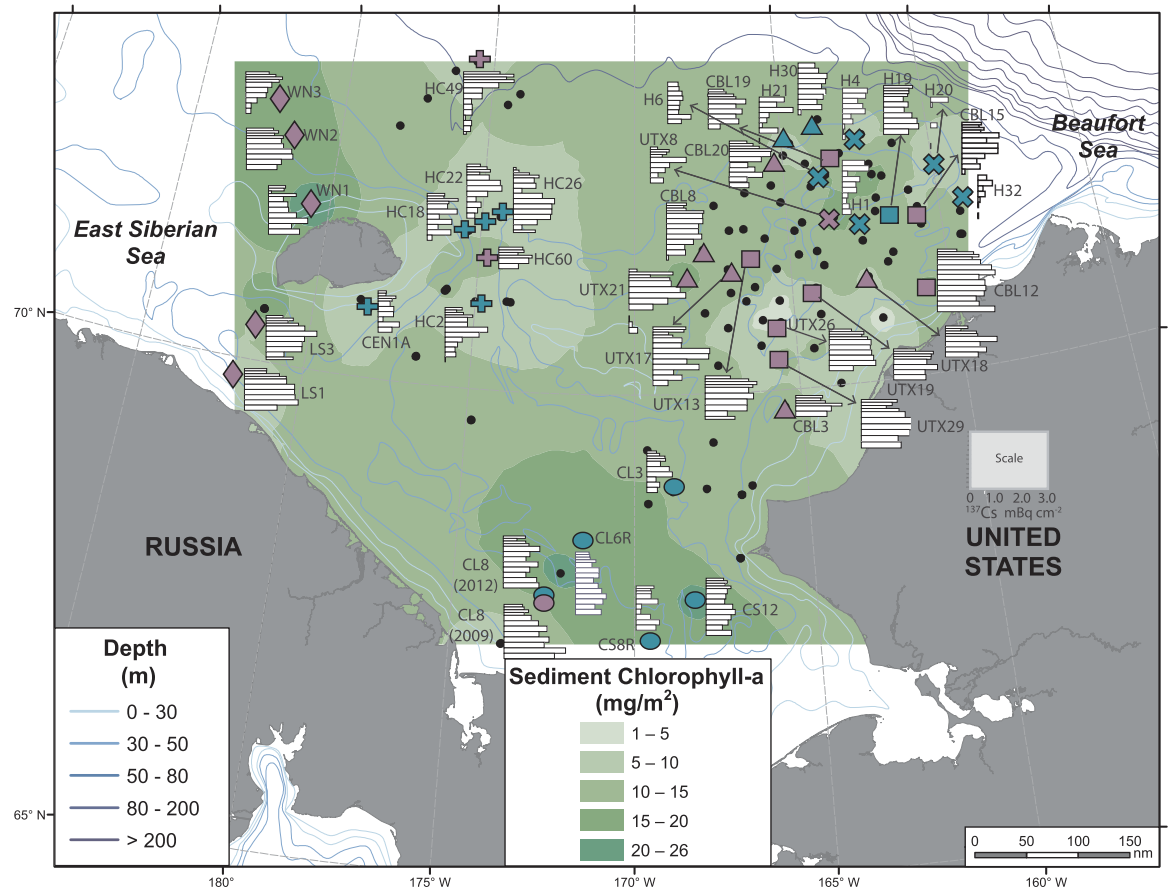

Fig. 14. Distribution of sediment chlorophyll in Chukchi Shelf surface sediments relative to miniaturized radiocesium profiles (units = mBq cm^{-2}) for the sediment cores reported here. Distributions of ^{137}Cs in the sediment profiles are plotted in detail with activity in units and standard errors on other individual figures. Symbol key and coloring scheme for symbols is the same as in Fig. 1.

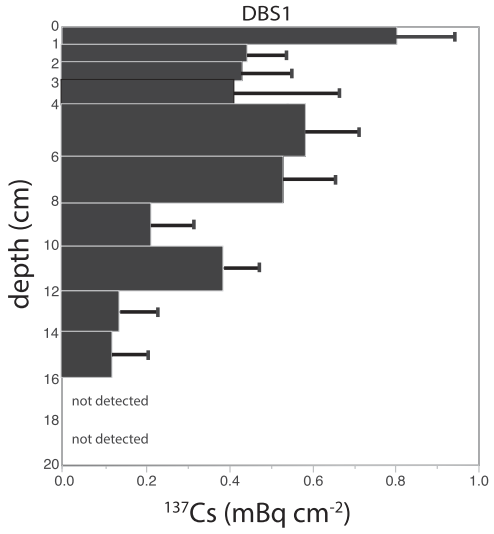

Fig. 15. Radiocesium distribution in a sediment core collected on the Bering continental slope (400 m water depth) 7 June 2007 during USCGC Healy Cruise no. 07–02. Station location is 60.0469°N, 179.6632°W.

radiocesium activity maximum from among the upper layers of the core where counting errors overlap, if we assume that the single highest subsurface peak for ^{137}Cs at 5 cm (Fig. 15) represents the 1963–1964 bomb fallout maximum, the 43.5 year period that had passed between the time this core was collected and the bomb fallout peak, results in an almost identical sedimentation rate of 0.12 cm $year^{-1}$.

Other sediment cores have been collected for radionuclide dating in the Bering Sea in recent years by Oguri et al. (2012). As was the case with our cores in the Chukchi Sea, this prior study did not find that ^{210}Pb decreased with depth in many of the cores, particularly those collected from shallow depths. Profiles of ^{137}Cs also showed a strong influence of bioturbation, as did an earlier study in the Bering Sea (Cooper et al., 1995). Surface sediment activities of radiocesium measured by Oguri et al. (2012) were in several cases non-detectable. We did not by contrast find any surface sediment where ^{137}Cs was not detected. However, total inventories of radiocesium, where detected, ranged from 5 to 67 mBq cm^{-2} (Oguri et al., 2012), which is comparable after accounting for radioactive decay to total core inventories reported for the Chukchi Shelf and Slope from sampling in 1993, which were 9 to > 40 mBq cm^{-2} (Cooper et al., 1998a).

The Oguri et al. (2012) study in the Bering Sea, as well as our efforts to compare sedimentation rates for ^{137}Cs and ^{210}Pb in the cores collected in 2009 and 2012 on the Chukchi shelf and adjoining areas of the East Siberian Sea demonstrate the complexity associated with evaluating sedimentation processes on biologically productive continental shelves with varying sediment composition. On the shallow shelf (typically < 60 m), bioturbation dominates or at least significantly alters sedimentation patterns recorded by radionuclide tracers such as ^{137}Cs and ^{210}Pb. The depth of sediment penetration of bomb fallout ^{137}Cs can reach 20 cm or more and bioturbation can be the dominant process where contaminants are spread evenly throughout this bioturbated layer. ^{210}Pb is an independent indicator of sedimentation, but application is more problematic because it requires a steady decrease in excess (background) ^{210}Pb downwards through the sediment core and not activities at any single depth. This is a more rigorous requirement

than the simple assumption that a maximum in ^{137}Cs represents the deposition that was concentrated at the time of the 1963–1964 bomb fallout peak that has since been re-distributed to some extent by bioturbation. In our study of 34 sediment cores for which both ^{137}Cs and ^{210}Pb data are available, only 14 cores, and the core collected on the Bering Slope in 2007 met the requirement for steady decreases in excess ^{210}Pb over the length of the sediment core (Fig. 8). Of the 14 cores meeting those criteria, in only 4 cases were the sedimentation estimates based upon ^{210}Pb reasonably consistent with sedimentation estimates from ^{137}Cs (Fig. 8, checked subplots). We defined reasonably consistent as differences of 0.02 cm year^{-1} or less in the sedimentation rate estimates independently provided by each radionuclide. However, small changes in the estimated slopes for ^{210}Pb or the depth of the ^{137}Cs maxima can alter significantly the estimated sedimentation rates. Given these uncertainties, even where there is agreement between the two methods, estimated sedimentation rates provided here should be used with caution for this continental shelf. The better agreement between the two radionuclide methodologies seen in the core sampled by Pirtle-Levy et al. (2009), as well as the Bering Slope core presented here are from cores collected from water depths (1496 m and 400 m, respectively), where bioturbation is clearly not dominant relative to sedimentation. It is possible, of course, that the ^{210}Pb sedimentation estimates obtained here are more accurate than those obtained from ^{137}Cs analyses, which are based upon the single point where a maximum was reached. However a broader point is simply the problematic challenge that is poised by needs to estimate sedimentation rates on biologically active shelves.

5. Conclusions

Despite the limitations inherent in applications to problems such as the expected persistence and penetration of contaminants in sediments on the broad arctic shelves, there are broad geographical patterns apparent in the distribution of radiocesium in sediments (Fig. 1). The depth of maximum activity, and the activity at that depth depends upon current flow, biological activity, and sedimentation and the combined interplay of those factors (Figs. 11 and 12). The intensity of the peak radiocesium activity is influenced by bioturbation (e.g. less intense and less prominent radiocesium maxima in the most productive benthic communities), and the depth of the radiocesium activity maximum is influenced by sedimentation. For example, deep and well-mixed ^{137}Cs inventories are observed in known areas of high benthic biological activities north of Bering Strait that also have high sedimentation. Current flow can limit overall deposition and reduce the depth of radiocesium distribution within the sediments through erosion of fine particles (e.g. Hanna Shoal and portions of Herald Canyon), as well as overall deposition. As better understanding is developed of biogeochemical processes on arctic shelves, e.g. Grebmeier (2012), and their productivity (Hill et al., this volume), the measurements of these two radioactive tracers, and probably other stable and radioisotopes show promise for helping to improve understanding of re-distribution mechanisms for biological and mineralogical materials in marine sediments.

Acknowledgements

This study is part of the Synthesis of Arctic Research (SOAR) and was funded in part by the U.S. Department of the Interior, Bureau of Ocean Energy Management, Environmental Studies Program through Interagency Agreement No. M11PG00034 with the U.S. Department of Commerce, National Oceanic and Atmospheric Administration (NOAA), Office of Oceanic and Atmospheric Research (OAR), Pacific Marine Environmental Laboratory (PMEL).

The field research was funded in part by the U.S. Department of the Interior, Bureau of Ocean Energy Management (BOEM), Alaska Outer Continental Shelf Region, Anchorage, Alaska under BOEM Cooperative Agreement No. M11AC00007 as part of the Chukchi Sea Offshore Monitoring in Drilling Area (COMIDA). Funding for the RUSALCA program was provided by NOAA. The Bering Sea core data collection and analysis was supported by the Bering Sea Project with funding from the National Science Foundation and the North Pacific Research Board. We thank the US Coast Guard crew and officers aboard the USCGC Healy, and crew and Captain of the RV Alpha Helix and RV Professor Khromov. COMIDA and RUSALCA colleagues helped with sample collection and we specifically thank our shipboard team, including Christian Johnson, Betty Carvellas, Mengjie Zhang, Laura Gemery, Dubrava Kirievskaya, Holly Kelly, Christina Goethel, and Piper Lewis. In addition, we thank Christian Johnson (assistance with gamma spectroscopy), and Alynne Bayard (GIS mapping and figure preparation). We thank John Trefry for assistance at sea with coring and for providing comments on an earlier version of the manuscript, and sharing additional unpublished data on sedimentation rates that helped put our results in context. Finally, we thank three anonymous reviewers who provided constructive comments that help improve the presentation and interpretation of the data, as well as the guest editorial team for their help in integrating the manuscript within this special issue.

References

Avery, S.V., 1996. Fate of caesium in the environment: distribution between the abiotic and biotic components of aquatic and terrestrial ecosystems. J. Environ. Radioact. 30, 139–171.

Baskaran, M., Naidu, A.S., 1995. ^{210}Pb-derived chronology, and the fluxes of ^{210}Pb and 137Cs isotopes into continental shelf sediments, East Chukchi Sea, Alaskan Arctic. Geochim. Et. Cosmochim. Acta 59, 4435–4448.

Beatty, W.S., Jay, C.V., Fischbach, A.S., Grebmeier, J.M., Taylor, R.L., Blanchard, A.L., Jewett, S.C., 2016. Space use of a dominant Arctic vertebrate: effects of prey, sea ice, and land on Pacific walrus resource selection. Biol. Conserv. 203, 25–32.

Bluhm, B., Iken, K., Hardy, S.M., Sirenko, B., Holladay, B., 2009. Community structure of epibenthic megafauna in the Chukchi Sea. Aqua. Biol. 7, 269–293.

Cooper, L.W., Grebmeier, J.M., Larsen, I.L., Solis, C., Olsen, C.R., 1995. Evidence for re-distribution of ^{137}Cs in Alaskan tundra, lake, and marine sediments. Sci. Total Environ. 161, 295–306.

Cooper, L.W., Grebmeier, J.M., Larsen, I.L., Dolvin, S., Reed, A.J., 1998a. Inventories and distribution of radiocessium in arctic marine sediments: influence of biological and physical processes. Chem. Ecol. 15, 27–46.

Cooper, L.W., Larsen, I.L., Beasley, T.M., Dolvin, S.S., Grebmeier, J.M., Kelley, J.M., Scott, M., Johnson-Pyrtle, A., 1998b. The distribution of radiocesium and plutonium in sea ice- entrained Arctic sediments in relation to potential sources and sinks. J. Environ. Radioact. 39, 279–303.

Cooper, L.W., Larsen, I.L., Grebmeier, J.M., Moran, S.B., 2005. Detection of rapid deposition of sea ice-rafted material to the Arctic Ocean benthos using the cosmogenic tracer ^{7}Be. Deep Sea Res. Part II: Top. Stud. Oceanogr. 52, 3452–3461.

Cooper, L.W., Grebmeier, J.M., Larsen, I.L., Egorov, V.G., Theodorakis, C., Kelly, H.P., Lovvorn, J.R., 2002. Seasonal variation in sedimentation of organic materials in the St. Lawrence Island polynya region, Bering Sea. Mar. Ecol. Prog. Ser. 226, 13–26.

Cooper, L.W., Savvichev, A.S, Grebmeier, J.M., 2015. Abundance and production rates of heterotrophic bacterioplankton in the context of sediment and water column processes in the Chukchi Sea. Oceanography 28, 84–99.

Crane, K., Ostrovskiy, A., 2015. Introduction to the special issue: Russian-American long-term census of the Arctic: RUSALCA. Oceanography 28, 18–23.

Cutshall, N.H., Larsen, I.L., Olsen, C.R., 1983. Direct analysis of ^{210}Pb in sediment: self-absorption corrections. Nucl. Instrum. Methods 206, 309–312.

Dunton, K.H., Schonberg, S.V., Cooper, L.W., 2012. Food web structure of the Alaskan nearshore shelf and estuarine lagoons of the Beaufort Sea. Estuar. Coasts 35, 416–435.

Dunton, K., 2015. Hanna Shoal: an integrative study of a high arctic marine ecosystem. Environ. Coast. Offshore Mag. 24–33.

Dunton, K.H., Grebmeier, J.M., Trefry, J.H., 2014. The benthic ecosystem of the northeastern Chukchi Sea: an overview of its unique biogeochemistry and biological characteristics. Deep Sea Res. Part II: Top. Stud. Oceanogr.

Dunton, K.H., Grebmeier, J.M., Trefry, J.H., 2017. Hanna Shoal: an integrative study of a High Arctic marine ecosystem in the Chukchi Sea. Deep Sea Res. Part II: Top. Stud. Oceanogr. 144, 1–5.

Fielding, P., Damstra, K.S.J., Branch, G., 1988. Benthic diatom biomass, production and sediment chlorophyll in Langebaan Lagoon, South Africa. Estuarine. Coast. Shelf Sci. 27, 413–426.

Grebmeier, J.M., Cooper, L.W., Feder, H.M., Sirenko, B.I., 2006. Ecosystem dynamics of the Pacific-influenced Northern Bering and Chukchi Seas in the Amerasian Arctic. Prog. Oceanogr. 71, 331–361.

Grebmeier, J., Cooper, L., 2014. PacMARS Sediment Chlorophyll-a. Version 1.0. UCAR/NCAR - Earth Observing Laboratoryhttp://dx.doi.org/10.5065/D6W9576K. (accessed 30 June 2017).

Grebmeier, J., Cooper, L., 2016. PacMARS Surface Sediment Parameters. Version 2.0. UCAR/NCAR - Earth Observing Laboratoryhttp://dx.doi.org/10.5065/D6416V3G.

(accessed 30 June 2017).
Grebmeier, J.M., 2012. Shifting patterns of life in the pacific arctic and sub-arctic seas. Annu. Rev. Mar. Sci. 4.
Grebmeier, J.M., McRoy, C.P., Feder, H.M., 1988. Pelagic-benthic coupling on the shelf of the northern Bering and Chukchi Seas. I. Food supply source and benthic biomass. Mar. Ecol. - Progress. Ser. 48, 57–67.
Grebmeier, J.M., McRoy, C.P., 1989. Pelagic-benthic coupling on the shelf of the northern Bering and Chukchi Seas. III. Benthic food supply and carbon cycling. Mar. Ecol. - Prog. Se. 53, 79–91.
Grebmeier, J.M., Bluhm, B.A., Cooper, L.W., Danielson, S., Arrigo, K.R., Blanchard, A.L., Clark, J.T., Day, R.H., Frey, K.E., Gradinger, R.R., Kedra, M., Konar, B., Kuletz, K.J., Lee, S.H., Lovvorn, J.R., Norcross, B.L., Okkonen, S.R., 2015. Ecosystem characteristics and processes facilitating persistent macrobenthic biomass hotspots and associated benthivory in the Pacific Arctic. Progress. Oceanogr. 136, 92–114.
Hargrave, B.T., 1973. Coupling carbon flow through some pelagic and benthic communities. Limnol. Oceanogr. 14, 801–805.
Hill, V., Ardyna, M., Lee, S.H., Varela, D.F., 2018. Decadal trends in phytoplankton production in the Pacific Arctic Region from 1950 to 2012. Deep Sea Res II. http://dx.doi.org/10.1016/j.dsr2.2016.12.015. (In press).
Jay, C.V., Fischbach, A.S., Kochnev, A.A., 2012. Walrus areas of use in the Chukchi Sea during sparse sea ice cover. Mar. Ecol. Progress. Ser. 468, 1–13.
Kanneworff, E., Nicolaisen, W., 1973. The "HAPS: " a frame supported bottom corer. Ophelia Suppl 10, 119–129.
Koide, M., Soutar, A., Goldberg, E.D., 1972. Marine geochronology with ^{210}Pb. Earth Planet. Sci. Lett. 44, 442–446.
Livingston, H.D., Bowen, V.T., 1979. Pu and ^{137}Cs in coastal sediments. Earth Planet. Sci. Lett. 43, 29–45.
Meyers, P.A., 1994. Preservation of elemental and isotopic source identification of sedimentary organic matter. Chem. Geol. 114, 289–302.
Moore, S.E., Grebmeier, J., 2017. The Distributed Biological Observatory: Linking Physics to Biology in the Pacific Arctic Region. Arctic in-press.
Noshkin, V., Bowen, V., 1973. Concentrations and distributions of long-lived fallout radionuclides in open ocean sediments. Pages 671-686 Radioactive contamination of the marine environment. IAEA Vienna.
Oguri, K., Harada, N., Tadai, O., 2012. Excess ^{210}Pb and ^{137}Cs concentrations, mass accumulation rates, and sedimentary processes on the Bering Sea continental shelf. Deep Sea Res. Part II: Top. Stud. Oceanogr. 61, 193–204.
Pirtle-Levy, R., Grebmeier, J.M., Cooper, L.W., Larsen, I.L., 2009. Chlorophyll a in Arctic sediments implies long persistence of algal pigments. Deep Sea Res. Part II: Top. Stud. Oceanogr. 56.
Pisareva, M.N., Pickart, R.S., Iken, K., Ershova, E.A., Grebmeier, J.M., Cooper, L.W., Bluhm, B.A., Nobre, C., Hopcroft, R.R., Hu, H.G., Wang, J., Ashjian, C.J., Kosobokova, K.N., Whitledge, T.E., 2015. The Relationship Between Patterns of Benthic Fauna and Zooplankton in the Chukchi Sea and Physical Forcing. Oceanography 28, 68–83.
Ritchie, J.C., McHenry, J.R., 1990. Application of radioactive fallout Cesium-137 for measuring soil erosion and sedment accumulation rates and patterns: a review. J. Environ. Qual. 19, 215–233.
Robbins, J.A., Edgington, D.N., 1975. Determination of recent sedimentation rates in Lake Michigan using Pb-210 and Cs-137. Geochim. Et. Cosmochim. Acta 39, 285–304.
Smith, J.N., Walton, A., 1980. Sediment accumulation rates and geochronologies measured in the Saguenay Fjord using the Pb-210 dating method. Geochim. Et. Cosmochim. Acta 44, 225–240.
Trefry, J.H., Trocine, R.P., Cooper, L.W., Dunton, K.H., 2014. Trace metals and organic carbon in sediments of the northeastern Chukchi Sea. Deep Sea Res. Part II: Top. Stud. Oceanogr. 102, 18–31.